AD-A133 659 RESEARCH AND DEVELOPMENT OF SUBSURFACE ACOUSTIC WAVE DEVICE CONFIGURATION..(U) UNITED TECHNOLOGIES CORP HARTFORD CT D E CULLEN ET AL. SEP 83 UTRC-R83-926157 1/1

UNCLASSIFIED AFOSR-TR-83-0825 F49620-82-C-0074 F/G 20/1 NL

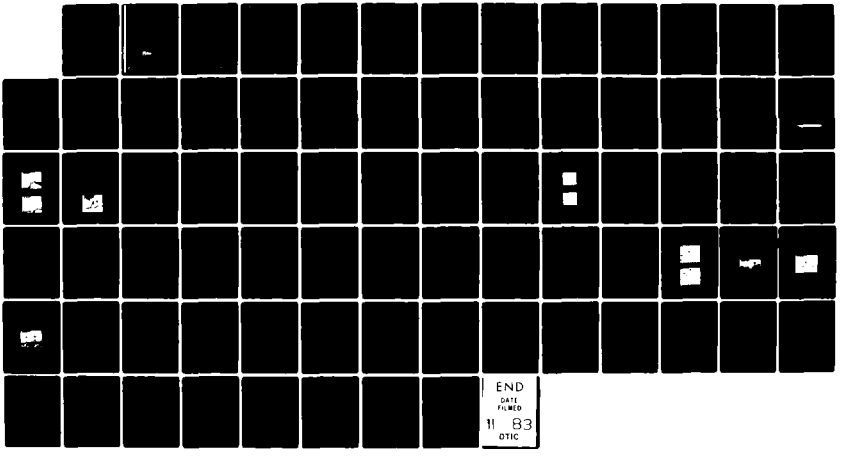

END
DATE FILMED
11 83
DTIC

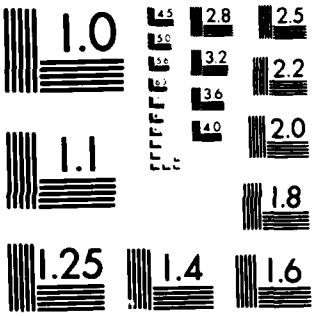

AFOSR-TR- 83-0825

(12)

RESEARCH AND DEVELOPMENT OF SUBSURFACE ACOUSTIC WAVE DEVICE CONFIGURATIONS FOR SENSOR APPLICATIONS

D.E. Cullen
G. Meltz
T.W. Grudkowski

Report No. R83-926157

Final Report Period Covered: July 15, 1982 — Sept. 12, 1983

Air Force Office of Scientific Research
Bolling AFB, D.C. 20332
Contract No. F49620-82-C-0074

UNITED TECHNOLOGIES RESEARCH CENTER

UNCLASSIFIED

SECURITY CLASSIFICATION OF THIS PAGE (When Data Entered)

REPORT DOCUMENTATION PAGE	READ INSTRUCTIONS BEFORE COMPLETING FORM
1. REPORT NUMBER: AFOSR-TR- 83-0825 / 2. GOVT ACCESSION NO.: AD-A133659	3. RECIPIENT'S CATALOG NUMBER:
4. TITLE (and Subtitle): Subsurface Acoustic Wave Device Configurations for Sensor Applications	5. TYPE OF REPORT & PERIOD COVERED: Final Technical Report July 1982 - Sept. 1983
	6. PERFORMING ORG. REPORT NUMBER: R83-926157
7. AUTHOR(s): Donald E. Cullen, Gerald Meltz, Thomas W. Grudkowski	8. CONTRACT OR GRANT NUMBER(s): F49620-82-C-0074
9. PERFORMING ORGANIZATION NAME AND ADDRESS: United Technologies Research Center, East Hartford, CT 06108	10. PROGRAM ELEMENT, PROJECT, TASK AREA & WORK UNIT NUMBERS: 61102F 2305/B2
11. CONTROLLING OFFICE NAME AND ADDRESS: Air Force Office of Scientific Research, Bldg. 410, Bolling Air Force Base, D.C. 20332	12. REPORT DATE: September, 1983
	13. NUMBER OF PAGES:
14. MONITORING AGENCY NAME & ADDRESS(if different from Controlling Office)	15. SECURITY CLASS. (of this report): Unclassified
	15a. DECLASSIFICATION/DOWNGRADING SCHEDULE

16. DISTRIBUTION STATEMENT (of this Report)

Approved for public release; distribution unlimited.

17. DISTRIBUTION STATEMENT (of the abstract entered in Block 20, if different from Report)

18. SUPPLEMENTARY NOTES

19. KEY WORDS (Continue on reverse side if necessary and identify by block number)

Acoustic Wave modes, Acoustic Wave Propagation

20. ABSTRACT (Continue on reverse side if necessary and identify by block number)

Subsurface acoustic wave modes that are sensitive to substrate strain but insensitive to temperature and surface fluid loading were sought for sensor applications. The properties of Stoneley-like interface waves in the layered structure $SiO_2/LiNbO_3$ were examined. A horizontal-shear surface wave in the same material configuration was found to be insensitive to surface fluids and was further studied for sensor applications. Zero first order temperature coefficients were found for these modes by varying the SiO_2 film thickness.

DD FORM 1 JAN 73 1473 EDITION OF 1 NOV 65 IS OBSOLETE

S/N 0102-LF-014-6601

UNCLASSIFIED

SECURITY CLASSIFICATION OF THIS PAGE (When Data Entered)

Block No. 20

Surface skimming bulk waves in quartz were also examined and found to possess the most attractive properties for continued work in acoustic wave sensor development.

ABSTRACT

Subsurface acoustic wave modes that are sensitive to substrate strain but insensitive to temperature and surface fluid loading were sought for sensor applications. The properties of Stoneley-like interface waves in the layered structure $SiO_2^{\square}/LiNbO_3^{\square}$ were examined. A horizontal-shear surface wave in the same material configuration was found to be insensitive to surface fluids and was further studied for sensor applications. Zero first order temperature coefficients were found for these modes by varying the $SiO_2^{\square}$ film thickness. Surface skimming bulk waves in quartz were also examined and found to possess the most attractive properties for continued work in acoustic wave sensor development.

ACKNOWLEDGEMENTS

The authors are pleased to acknowledge the individuals who made important contributions during the course of this program. A. J. DeMaria and G. K. Montress provided program management with helpful suggestions and guidance to the technical effort. R. Basilica fabricated all of the experimental devices. S. Sheades assisted in the measurement of device characteristics. Prof. E. L. Adler of McGill University made the initial multi-layer computer code available, and M. Page assisted in the modification of the code to adapt it to our use.

TABLE OF CONTENTS

R83-926157

Research and Development of Subsurface Acoustic Wave Device Configurations for Sensor Applications

1.0 INTRODUCTION

1.1 Program Objectives and Goals

The research and development program conducted by United Technologies Research Center (UTRC) was directed toward the theoretical and experimental understanding of the basic propagation characteristics of subsurface acoustic waves (SSAW) in materials appropriate for practical SSAW sensors. The principle objectives of the program were to identify promising propagation mode and substrate configurations and then to experimentally determine the propagation characteristics that are relevant to SSAW sensor development. Strain sensitivity, temperature sensitivity, coupling efficiencies, and propagation losses were among the more important characteristics determined. Materials and modes that give rise to high strain sensitivity and low temperature sensitivity were sought. The primary goal of the program was to determine one or more SSAW structures whose properties are attractive for the development of a low cost SSAW accelerometer or other sensors.

1.2 Technical Approach

Surface acoustic wave (SAW) devices, in which Rayleigh waves propagate on the surface of a piezoelectric crystal, are finding ever increasing use as delay lines, filters and a wide range of signal processing devices. Their low loss, small size, and the fact that the surface nature of the wave provides access to the entire propagation path are important advantages of SAW devices. Precision, frequency output SAW sensors have been demonstrated using these SAW oscillators. However, because SAW devices are very sensitive to surface contamination, their use in sensors, where a high degree of stability is required over extended periods of time, leads to severe packaging problems. Subsurface acoustic waves which propagate beneath, but within a few wavelengths of the surface, have been shown to minimize or eliminate the contamination problem and are, therefore, an attractive alternative for acoustic wave sensor applications. During the course of this program, the properties of several SSAW modes have been examined, and one of these modes is strongly recommended for further study for sensor applications.

A variety of different types of SSAW's are possible. Stoneley waves, probably the oldest known type of subsurface wave (Ref. 1), propagate along the interface between two materials with the acoustic energy concentrated in a narrow region a few wavelengths wide about the interface. Unfortunately, the conditions under which Stoneley waves exist are very restrictive, and it is only very recently that Stoneley waves have been considered experimentally for device applications. Yamanouchi and co-workers at Tohoko University in Japan (Ref. 2,3) studied the propagation characteristics of Stoneley Waves in 126° rotated Y-cut, X-propagating $LiTaO_3$ with an amorphous SiO_2 film overlay. They also mentioned, but gave no results for SiO_2/128°YX $LiNbO_3$.

Acoustic waves may also be confined to the interface region between two materials by placing a thin layer of a third material with a lower acoustic velocity at the interface. One example of this kind of guided interface wave is found in Ref. 4, where a study of acoustic waves guided by a thin fluid layer between two solids is reported. Interface waves in ZnO/Au/Si layered structures were demonstrated earlier at UTRC. In this case the ZnO film provided the piezoelectric coupling and the thin Au film was the "slow" layer that confined the acoustic wave to the interface. This type of guided interface wave is thought to exist for many material combinations and thus should prove more useful than the Stoneley wave for sensor applications.

A third type of SSAW that is of interest is the surface skimming bulk wave (SSBW). Discovered in 1977 (Refs. 5,6), this type of wave has since been reported in several cuts of quartz, in $LiNbO_3$ and in $LiTaO_3$ (Ref. 7). The wave is launched from an interdigital transducer (IDT) much like a Rayleigh wave, but propagates at a shallow angle to the surface, and may be detected by a second IDT located downstream from the launching IDT. SSBW devices with a zero first-order temperature coefficient have been reported for rotated Y-cut quartz substrates (Ref. 8). The SSBW is unlike the Stoneley and interface waves in that no dielectric film overlay is required and the waves are launched and detected at the surface. However, unlike Rayleigh waves, SSBW's are horizontally polarized shear waves. The sensitivity to surface fluid loading is far less than that of a Rayleigh wave since the shear horizontal (SH) wave does not radiate compressional waves into the surface fluid. The level of sensitivity of SSBW's to fluid loading was studied during the program. Figure 1-1 illustrates schematically the substrate configurations for the three types of SSAW's just described.

1.3 Description of Program Tasks

The program was a research effort that was divided into two major tasks. In task I, candidate materials and propagation modes were selected. Devices were fabricated and tested to confirm SSAW propagation. Extensive measurements of propagation characteristics were performed in Task II. The purpose and goals of Tasks I and II were as follows:

Task I - Selection and Confirmation of Candidate SSAW Configuration

Candidate SSAW configurations were selected after a careful review of the literature and of UTRC's own work in the field. The selection of candidates, and in particular, the determination of the appropriate substrate crystallographic orientations, was assisted by UTRC's analytical modeling capabilities. Because the guided acoustic wave mode and the surface skimming bulk wave mode were thought to offer the most potential for temperature compensated sensors, these modes were to be emphasized. Nevertheless, at least one Stoneley wave configuration was to be examined. Sample devices of each configuration were fabricated and SSAW propagation confirmed. The effects of variations in electro-acoustic transducer design, overlay film thicknesses, film deposition conditions, and substrate crystallographic orientation were examined in order to develop low-loss SSAW devices with minimum sensitivity to surface contamination. The goal of Task I was to identify configurations that offered promise for the development of a SSAW accelerometer or other SSAW sensor, and, at least four (4) such configurations were to be selected for extensive testing in Task II.

Task II - Experimental Characterization of SSAW Sensor Configurations

The SSAW propagation characteristics which are important to the development of a SSAW sensor were determined for those configurations selected in Task I. At least two (2) devices of each configuration were fabricated and measured for: 1) strain sensitivity, 2) temperature sensitivity, 3) electro-acoustic transduction efficiency, 4) propagation loss, and 5) sensitivity to surface contamination. The use of a SSAW device as a sensor is based upon the sensitivity of SSAW propagation to substrate strains, and in particular, to bending strains. In view of this, UTRC's strain sensitivity measurements were carried out using a pure bending strain configuration, and strain sensitivities were determined for strains both parallel and perpendicular to the direction of SSAW propagation. Temperature sensitivities were to be measured on unstressed devices over the entire -50°C to +125°C temperature range. In guided acoustic wave devices, where there is some freeedom in the choice of substrate, metal film, and dielectric film overlay materials, variations in material combinations were examined in an effort to develop SSAW configurations with minimum temperature sensitivity. The goal of Task II was to determine, by experimental measurement of device characteristics, one or more SSAW configurations whose properties are attractive for the further development of a low cost SSAW accelerometer or other SSAW sensor, and to assess prototype sensor performance capabilities.

1.4 Summary of the Report

The following section describes the experimental and theoretical methods utilized in the performance of these tasks. Sections 3, 4, and 5 describe the detailed configurations and results achieved for several SSAW device geometries considered. A summary and recommendations for continued developments in Section 6. This program has resulted in considerable advancement of fundamental knowledge concerning the properties of subsurface acoustic waves and has resulted in a clear understanding of criteria for achieving device configurations and material characteristics suitable for sensor and other device applications.

During the course of the program, a paper entitled "Surface and Interface Acoustic Waves In SiO_2/YX-$LiNbO_3$" has been submitted to Applied Physics Letters and is included in this report as Appendix A. Presentation of initial results was made at the 1982 IEEE Ultrasonics Symposium in a paper entitled " "Investigation of the Strain Sensitivity of Subsurface Acoustic Wave Modes". Further material contained in this report is being considered for additional publication.

2.0 Experimental and Theoretical Methods

2.1 Selection of Device Configurations

A review of the relevant literature showed that the group at Tohoko University (Ref. 2,3) have been the only researchers to investigate Stoneley waves in piezoelectric materials, and that there have been no reports of work on guided interface waves in any configuration of interest. Surface skimming bulk Baves have been studied extensively, but primarily for high frequency oscillator applications. Their sensitivities to substrate strain and surface fluid loading, two pieces of information necessary for sensor design, are not available in the literature.

The only known material configuration that is piezoelectric and satisfies the Scholte (Ref. 9) Stoneley mode existance conditions (see Fig. 2-1) is the $SiO_2/126^oYX\text{-}LiTaO_3$ structure. On an earlier AFWAL program (Contract No. F33615-80-C-2044) this structure was examined at UTRC and the results of Ref. 2 and 3 confirmed at SiO_2 thicknesses of $h = 2\lambda/3$ and $h = \lambda$. Strain sensitivities both parallel and perpendicular to the direction of acoustic wave propagation were measured and found to be very low. In addition, the $LiTaO_3$ substrates were costly and very difficult to process due to their high sensitivity to thermal gradients and susceptability to brittle fracture at low strain levels. As as result, this configuration is considered unsuitable for sensor applications.

It would appear, from Fig. 2-1, that the $LiNbO_3$ slow shear-wave velocity configuration, $SiO_2/128^oYX\text{-}LiNbO_3$, analogous to the above $LiTaO_3$ structure, does not quite fall into the allowed region for Stoneley waves. However, small changes in the SiO_2 film density or shear modulus could shift the point in Fig. 1-2 to within the allowed region. Also, the Scholte existence conditions were derived for isotropic media and, therefore, do not strictly apply in the present case. In an early abstract to Ref. 3, it was stated that this $LiNbO_3$ structure exhibits acoustic modes similar to those found in the $LiTaO_3$ devices. As a result, it was decided to investigate the $SiO_2/128^oYX\text{-}LiNbO_3$ configuration for Stoneley waves.

Reports in the literature on guided interface waves in the solid-liquid film-solid configurations and early success at UTRC with ZnO/Au/Si devices gave rise to the hope that such waves could be obtained with a wide variety of material combinations. In that case, the materials could be chosen to optimize the device for high strain sensitivity and low thermal sensitivity. From work at UTRC (Ref. 10) and elsewhere (Ref. 11) it is known that a zero value of the first-order temperature coefficient (TC) can be obtained with SAW devices by overlaying the SAW substrate with a dielectric film. The dielectric material is chosen to have a TC that is opposite in sign to that of the substrate, and at the proper film thickness, the TC can be reduced to zero. Since there is no prior knowledge of how to maximize strain sensitivity in these layered structures, it was decided to investigate a substrate-film combination with TC's of opposite sign. The zero TC film thickness would be found and the strain sensitivity determined at that point. The combination of a Y-cut-$LiNbO_3$ substrate and a SiO_2 film, with an intervening Au film as the "slow" layer was selected. Other materials could have been chosen for this study, however, of the common crystalline piezoelectrics, only $LiNbO_3$, quartz, and possibly GaAs can be considered suitable for sensor applications where mechanical properties are important considerations. $LiNbO_3$ was chosen

for the guided interface wave study because of its very high piezoelectric coupling coefficient and because it was assumed that a zero TC could be obtained with the SiO_2 film-$LiNbO_3$ substrate combination.

For an investigation of strain sensitivity and surface fluid loading in SSBW devices, quartz was the obvious choice. It is the only SSBW crystalline material which exhibits a zero first order TC, and its mechanical properties are unsurpassed as evidenced by its wide use in crystal oscillators and other electro-mechanical devices.

2.2 Measurement of SSAW Propagation Characteristics

The properties of SSAW devices that are most important for sensor design are strain and temperature sensitivity. We have sought configurations that produce high strain sensitivity and minimum temperature sensitivity. Also important are the electroacoustic properties such as transducer coupling efficiency and propagation loss. Excessive losses in any portion of the device are, of course, undesirable. Above all, the SSAW device must be unsensitive to conditions on the surfaces of the substrate to be considered for sensor applications.

Because SSAW devices are similar to SAW devices as far as the measurement of their characteristics is concerned, it is unnecessary to describe here the standard techniques used to measure electroacoustic properties. Measurement of temperature sensitivity is also straightforward. There are several ways to make these measurements, and one that has been found convenient and reliable is to form an oscillator with the acoustic device and track the oscillator frequency versus temperature. Such measurements are performed routinely at UTRC with a computer controlled facility dedicated to characterizing devices versus temperature and/or pressure. The sensitivity of SSAW propagation modes to surface fluid loading was determined by immersing the device into a silicone oil and monitoring the change in insertion loss.

The strain sensitivity of a SSAW device can be thought of as a sum of two effects: 1) the physical change in the length of the propagation path, and 2) the change in the SSAW propagation velocity with substrate strain. To first order, the strain dependence of the SSAW velocity can be written

$$v = v_o (1 + \gamma_j S_j) \qquad (2\text{-}1)$$

where S_j are the strains in abbreviated subscript notation, v_o is the velocity in the unstrained state, and γ_j are the set of strain coefficients for the particular SSAW configuration. The S_1 and S_2 components of normal strain are taken to be the strain in the plane of the substrate parallel and transverse to the direction of SSAW propagation while S_3 is the strain perpendicular to the surface of the substrate. Since shear strains must vanish at a free surface, and the S_3 component of normal strain is usually quite small compared to S_1 and S_2, the strain dependence of SSAW waves will be represented by

$$v = v_o (1 + \gamma_1 S_1 + \gamma_2 S_2) \qquad (2\text{-}2)$$

Values of γ_j are known for bulk acoustic waves in many solids and for SAW waves in a few materials.

The strain sensitivity of SSAW devices was measured using a technique adapted from earlier work on SAW devices (Ref. 12). The experimental setup for these measurements is shown schematically in Fig. 2-2. A pure bending state of strain is created in the substrate in the region between the inner set of dowel pins. The 2:1 ratio between the width of the substrate and the distance between the two central dowel pins insures that the state of strain in the central portion of the substrate is truly one of pure bending (Ref. 13). Substrates fitted with strain gages were used to experimentally check the state of strain. The results showed: 1) that the bending strain at the surface could be deduced from a knowledge of the geometry of the substrate and the loading fixture and the magnitude of the applied load, and 2) that there were no measurable transverse strains.

To determine the strain sensitivity, an oscillator is created with the SSAW delay line and the change in oscillator frequency, f, recorded as a function of applied load, F. Because the state of strain is uniform and unidirectional over the SSAW path, simple equations can be derived relating the strain coefficients γ_1 and γ_2 to the slope of the frequency versus strain data (Ref. 12). These relations are

$$\gamma_1 = 1 + \frac{1}{f}\frac{\Delta f}{\Delta S_1}, \text{ and } \gamma_2 = \frac{1}{f}\frac{\Delta f}{\Delta S_2} \qquad (2\text{-}3)$$

where S_1 and S_2 are the bending strains parallel and perpendicular to the SSAW propagation direction. While the bending state of strain produced by the loading arrangment of Fig. 2-2 is uniform over the area of the SSAW device, the strain varies linearly with distance into the substrate. Unless the substrate thickness is very large compared to the acoustic wavelength, or the strain variation is properly accounted for, the experimental values of γ_1 and γ_2 obtained can be significantly in error. In strain measurements made during this program, the substrates were typically 30λ thick, holding errors to less than 10 percent (Ref. 14). For purposes of preliminary device evaluation, errors of this magnitude are tolerable.

The relationship between the appplied load, F, and the strain components, S_1 and S_2 were arrived at as follows. Let the width and thickness of the substrate be w and t, respectively, and the distance between the upper and lower loading pins be d. The bending stress at the upper surface of the substrate in the region between the two central dowel pins is then given by $T = (3d/w)(F/t^2)$. For Y-cut or rotated Y-cut substrates, and the simple state of strain generated by the pure bending loading configuration, $T_X = C_{11}S_X$, $T_Z = C_{33}\,S_Z$ and $T_Z^1 = C^1_{33}\,S_Z^1$ where T_X, T_Z are the normal stresses in the X, Z directions for Y-cut substrates and T_X, T_Z^1 are the normal stresses in the X,Z^1 directions for rotated Y-cut substrates (Z^1 is in the plane of the substrate). The strains in the X,Z, and Z^1 direction are S_X, S_Z and S_Z^1 and C_{11}, C_{33} and C_{33}^1 are the appropriate elastic constants. For the quartz and $LiNbO_3$ substrates employed in this work, the appropriate constants are given in Table 2-1.

Experimentally, this technique for determining the strain coefficients is simple and the results unambiguous. Earlier SAW strain sensitivity measurements made on quartz yielded coefficients which agreed closely with subsequent theoretically derived values (Ref. 15).

2.3 Interface Modes in Multilayer Media

Theoretical Models

There are several systematic procedures for determining the velocities and characteristics of straight-crested, guided modes in stratified surface-wave configurations (Refs. 16-18). From a mathematical prespective, these techniques are all equivalent to finding the complex eigenvalues of an assembly of translationally invariant structures. In one method, the solution is obtained from a superposition of partial waves chosen to satisfy continuity conditions at the layer interfaces and free (or shorted) surface boundary conditions at the top-most layer. An alternative method is known as the transfer matrix technique. In this procedure, the eigenvalue problem is formulated in terms of a mode state vector and transfer matrices that relate the state vector in the substrate to its value anywhere in the layered structure. This method if preferable because it is computationally more tractable. Regardless of the number of layers, it requires at most the setting of a 5 x 5 determinant to zero to satisfy all the mechanical and electrical boundary conditions.

A clear exposition of the transfer matrix approach was given by Fahmy in his thesis on acoustic wave propagation in multilayer media (Ref. 18), and by B. Kennett in his recent articles (Ref. 17). A description of the mathematical techniques are given in the following section. The approach in the present work closely follows that of Fahmy.

Mathematical Formulation

Consider a multilayer structure composed of a semi-infinite half-space (the substrate) and k layers of finite thickness anisotropic, possibly piezoelectric, plates. These layers can be in direct contact or have interposed a thin metallic layer. The coordinate system is aligned with the X_1 axis along the direction of propagtion parallel to the interfaces and the outward surface normal X_3 (cf. Fig. 2-3). The substrate is defined by $X_3 \leq 0$. All of the elastic and electrical properties of the layers are expressed in these coordinates by suitable rotations of the constitutive tensors, such as the compliance, permittivity, piezoelectric stress, etc., from crystal axes to the layer axes.

Referring to the axes X_1, X_2, X_3, the constitutive equations are

$$T_{ij} = C_{ijk\ell}\, u_{k,\ell} + e_{\ell ij}\, \varphi_{,\ell} \qquad (2\text{-}4)$$

$$D_j = e_{jk\ell}\, u_{k,\ell} - \varepsilon_{j\ell}\, \varphi_{,\ell} \qquad (2\text{-}5)$$

and the equations of motion and Gauss's law become

$$\rho \ddot{u}_i = T_{ij,j} \tag{2-6}$$

$$D_{j,j} = 0 \tag{2-7}$$

where

T_{ij}	=	stress tensor
u_k	=	displacement vector
D_j	=	electric displacement vector
φ	=	electric potential
$C_{ijk\ell}$	=	compliance tensor
$e_{\ell ij}$	=	piezoelectric stress tensor
$\varepsilon_{j\ell}$	=	permittivity tenso.

Repeated indices denote summations and a "comma" subscript stands for differentiation with respect to the coordinate shown by the subscript following it.

These equations can be made more compact by defining the following vectors and matrices (by taking advantage of the inherent symmetry in the constitutive relations)

$$T^j \equiv [T_{ij}] \quad , \text{ 3 x 1 vector}$$

$$C^{j\ell} \equiv [C_{ijk\ell}] \quad , \text{ 3 x 3 matrix}$$

$$\xi^{j\ell} \equiv [e_{\ell ij}] \quad , \text{ 3 x 1 vector}$$

$$U \equiv [u_k] \quad , \text{ 3 x 1 vector}$$

Using these definitions, Eqs. (2-4) and (2-6) simplify to

$$T^j = C^{jl}\, U_{,\,l} + \xi^{jl}\, \phi_{,l} \tag{2-8}$$

$$-\omega^2\, \rho\, U = T^j{}_{,l} \tag{2-9}$$

for a time dependence of exp ($-i\omega t$). Now assume a spatial dependence of the form exp ($\lambda_i\ X_i$) where λ is the propagation vector wave number with components λ_i, i = 1, 2, 3. By eliminating T^1 and T^2 from Eq. (2-8) and Eq. (2-9) and noting that differentiation with respect to the "ith" coordinate is equivalent to multiplication by λ_i, we can (after considerable algebra) cast Eqs. (2-5, 8 and 9) into a matrix eigenvalue equation:

$$[\lambda_3 I - A_3]\ \tau^3 = 0 \tag{2-10}$$

where τ^3 is an 8 dimensional mode state vector,

$$\tau^3 = [T^3,\ D_3,\ U,\ \ ]^t$$

and A_3 is an 8 x 8 system matrix that depends on the material constants, ω and λ_1 (if the mode varied perpendicular to the sagital plan then A would also depend on λ_2). Equation (2-10) is equivalent to the matrix differential equation

$$\partial\tau^3/\partial X_3 - A_3\tau^3 = 0 \tag{2-11}$$

Since A_3 is space invariant, there exists a matrix exponential function that transfers the state vector τ^3 from an arbitrary origin within a layer (or the substrate) to a point h a[illegible]g the X_3 axis. Thus the solution to Eq. 2-11 is given by

$$\tau^3(h) = \phi^3(h)\ .\ \tau^3(0) \tag{2-12}$$

where

$$\phi^3(h) = \exp\ [A_3 h] \tag{2-13}$$

is the layer or substrate transfer matrix.

Consider an infinite plate of thickness, h, at each free surface (open circuit) the stress and electric displacement components of τ^3 vanish, thus

$$\tau^3(h) = \Phi^3(h)\ \tau^3(0) = 0 \tag{2-14}$$

which for a non-trival solution requires

$$|\Phi^3(h)| = 0 \tag{2-15}$$

Only the upper right quarter of the 8 x 8 transfer matrix is needed in Eq. (2-15) since the first four components of the continuous state vector τ^3 vanish at both interfaces. The solution(s) to Eq. (2-15), and thus the allowed plate modes, are found by varying the propagation velocity (along X_1) until Eq. (2-15) is satisfied to within some predetermined tolerance.

In the case of a half-space (or substrate) defined by $X_3 \leq 0$, it is convenient to represent τ^3 in terms of a linear combination of eigenmodes. If P is a modal matrix (Ref. 19) for A_3, then the system vector of the substrate is given by

$$Y^3 = P^{-1}\ \tau^3 \tag{2-16}$$

The 8 x 1 vector Y^3 is the projection of τ^3 on the vector space defined by the eigenmodes of A_3. If $\Lambda = P^{-1} A\ P$ is the diagonal matrix whose elements are the eigenvalues of A_3, then

$$Y^3\ (X_3) = \exp\ (\Lambda\ X_3)\ Y^3\ (0) \tag{2-17}$$

This follows from Eqs. (2-11) and (2-16) upon noting that $P^{-1}\ P = I$. At the free surface, T^3 and D_3 vanish so that the boundary condition becomes

$$[\tau^3(0)]_U = [P]_U\ Y^3(0) = 0 \tag{2-18}$$

where the subscript U denotes the upper half of the vector or the matrix. For a non-trivial solution,

$$|[P]_U| = 0 \tag{2-19}$$

The modal matrix P is an 8 x 8 matrix of eigenvectors corresponding to the eigenvalues of A_3. Generally, one only retains those eigenmodes which decay into the substrate and thus P can be reduced to a smaller matrix. For example, in the case of a generalized surface wave no more than 4 eigenmodes are required to represent the mode state vector.

If the substrate is overlaid with k layers of finite thickness, then it follows from the preceeding discussion that

$$[\tau^3_{\text{Free Surface}}]_U \left[\prod_{i=1}^{k} \phi_i^3\right]_U \cdot PY^3 = 0 \tag{2-20}$$

and for non-trivial solutions

$$\left|\left[\prod_{i=1}^{k} \phi_i^3\right]_U \cdot P\right| = 0 \tag{2-21}$$

This determinant, which is 4 x 4 in this case, is a complex transcendental function of the frequency f, the wave velocity v and the attenuation . Equation (2-21) takes the form

$$F(f, z) = 0 \tag{2-22}$$

where $z = i\omega/(v_o \lambda_1)$ is a normalized complex wavenumber and v_o is a judicious guess at the value of the wave velocity v. The entire problem is now reduced to determining the complex roots of Eq. (2-22). The roots are found by searching about z = 1 for the minimum of

$$W(f,z) \equiv |\text{Re}(F)| + |\text{Im}(F)| \tag{2-23}$$

since the zeros of W are the zeros of F. Moreover, the maximum modulus theorem states that all concave upward regions in the surface W contain zeros since the function has no minimum other than W = 0.

The transfer matrix technique is a powerful general method for analyzing elastic waves in complex layered media, and was employed in the investigation of such structures in the present program.

In Section 3, 4, and 5, detailed experimental and theoretical work is described for the several SSAW configurations investigated.

Table 2-1

Elastic Constants

Material	Cut Angle	C_{11}	C_{33}	C'_{33} ($\times 10^6$ psi)
Quartz	-36°	12.6		14.1
	-42.75°	12.6		10.9
$LiNbO_3$	0°	29.4	35.5	
	128°	29.4		28.6

STONELEY WAVE EXISTENCE REGIONS

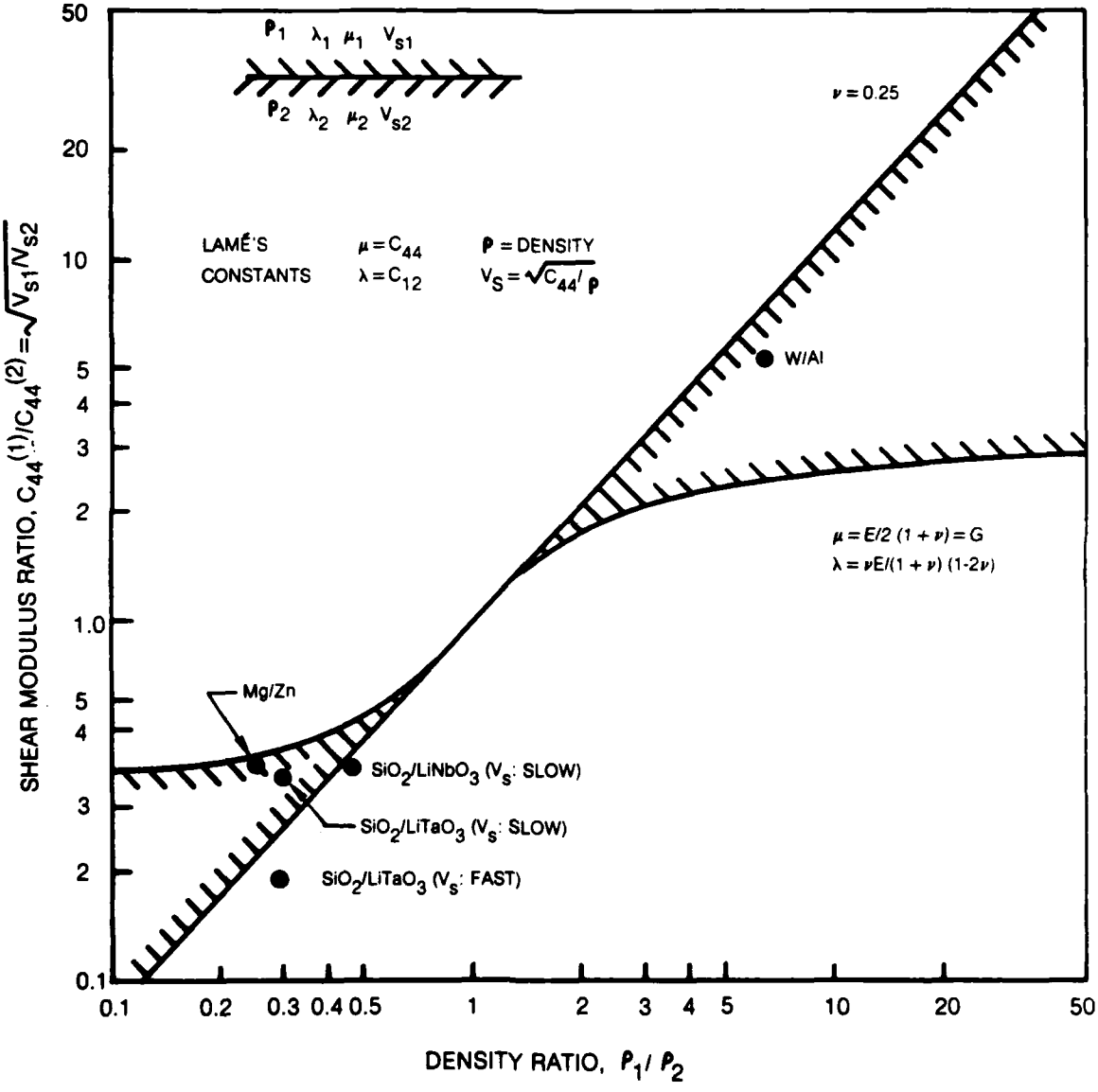

83-8-12-4

FIG. 2-2

STRAIN SENSITIVITY EXPERIMENT

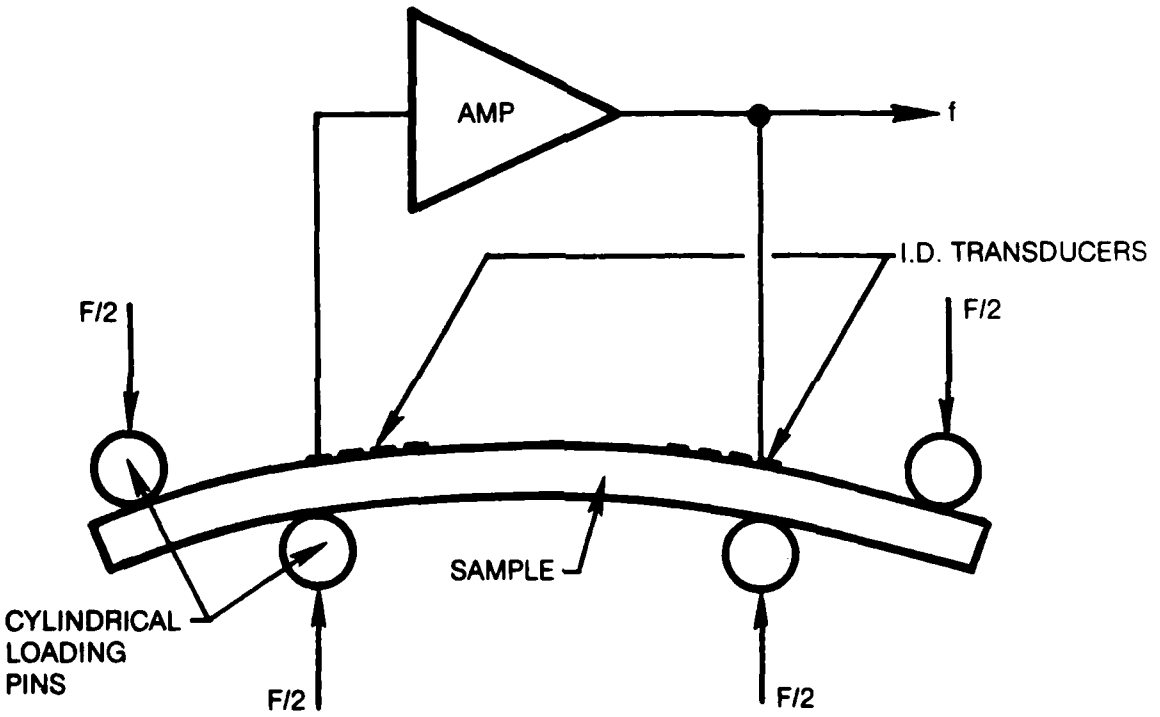

83-8-12-2

TYPICAL MULTILAYER STRUCTURE

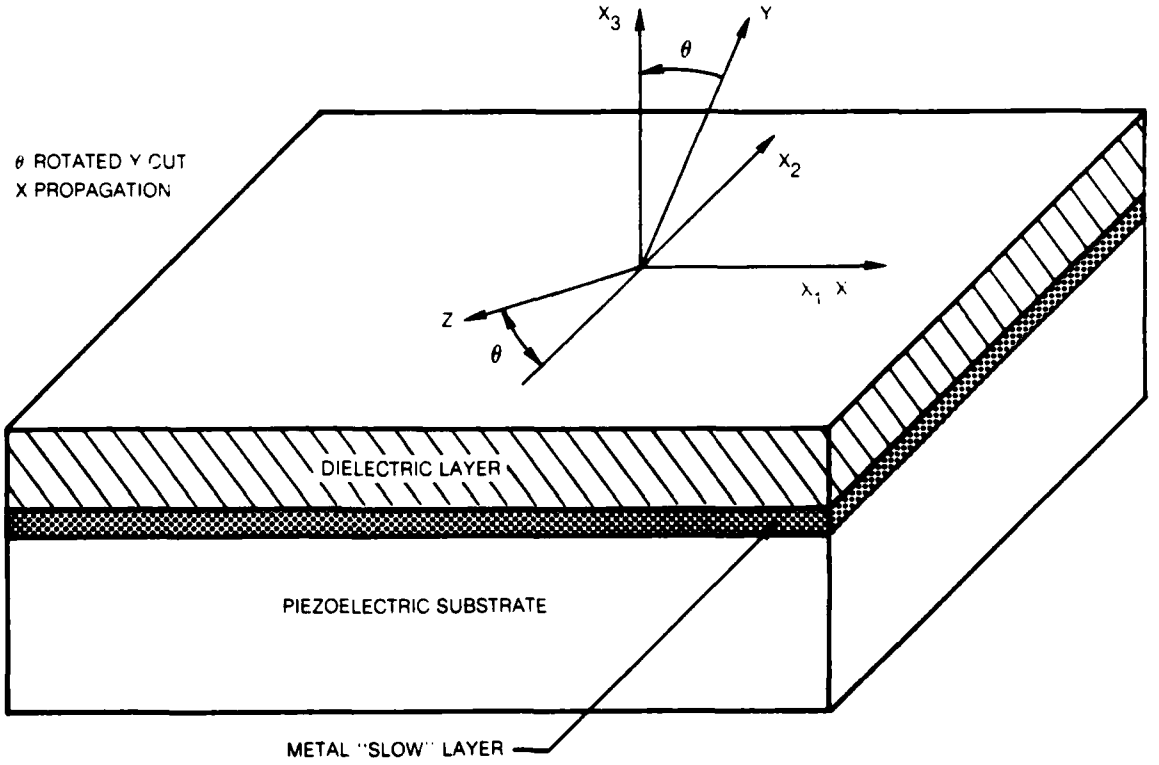

3.0 Surface Skimming Bulk Waves in Quartz

Figure 3-1 shows the quartz substrate configuration which: 1) supports a surface skimming bulk wave (SSBW) acoustic mode, and 2) exhibits a zero first order temperature coefficient. This configuration is defined by the Y-crystalline axis having a 36° rotation relative to the surface normal. SSBW propagation is perpendicular to the X-direction. The SSBW is a type of subsurface acoustic wave (SSAW) which is radiated at a shallow angle into the substrate. The acoustic particle motion is shear horiztonal (SH). Unlike surface waves or guided wave modes, the SSBW wave motion versus depth into the substrate is determined by the launching interdigital transducer (IDT) electrode pattern and its depth into the substrate increases as the wave propagates. Thus, the wave is actually a bulk shear wave which, because of the crystalline orientation, is launched into the substrate with a field distribution similar to that determined by an end-fire array, i.e., the IDT. A calculated far-field SSBW radiation pattern (Ref. 20) is sketched in Fig. 3-1.

The frequency response of a SSBW delay line is shown in Fig. 3-2 where the insertion loss at the fundamental frequency and third harmonic frequency of a representative device are presented. As in the case with surface waves, double electrode transducers have nearly the same efficiency in launching fundamental and third harmonic SSBW's and operation at the third harmonic may be desirable from a strain sensitivity standpoint as will be explained below.

Several delay line designs were used in the present program and Table 3-1 lists the important parameters of the various designs. The data for Fig. 3-2 was obtained from a DL1 type device. Because the DL1 pattern was not optimized for SSBW's, the insertion loss (IL) minimum in Fig. 3-2 is rather high (30 dB). Values of IL as low as 8.2 dB were obtained with SSBW devices fabricated using the DL11 pattern, and even lower IL can be obtained if required. A portion of the follow-on effort will be devoted to optimizing the SSBW IDT design.

Examples of the sensitivity of the IL characteristic to surface fluid loading are given in Fig. 3-3. The double exposures of IL versus frequency show the increase in loss that occurs upon immersing the entire delay line in a silicon oil. Because a SSBW is a horizontally polarized shear wave, and since shear waves cannot propagate in a non-viscous liquid, it was conjectured that the losses resulting from immersion of a SSBW device in a low viscosity fluid might be acceptable. Figure 3-3 shows a $\lambda = 16$ μm, DL11 device which incurred an additional loss of 11 dB when immersed in oil and a longer wavelength DL1 deice whose IL increased by 4 dB. The maximum increase in IL due to fluid loading for all SSBW devices tested was 12 dB. For a SSBW device with an initial IL of about 10 dB or less, which is easily achieved, the additional loss due to oil immersion is quite tolerable. From an IL standpoint, practical sensors may be achieved with SSBW delay lines.

The temperature characteristics of SSBW devices on 36° rotated Y-cut quartz substrates are particularly attractive for sensor development. Figure 3-4 shows the measured frequency versus temperature behavior of such a device. An acoustic wave oscillator is formed with the SSBW device in the feedback loop of an amplifier controlling the frequency of oscillation. Such an oscillator is then placed in a temperature chamber and the frequency recorded as a function of temperature. Figure 3-4 shows that the device has a zero first order temperature coefficient of delay at T_0 = 39.03°C, and that the second order coefficient $\alpha = 7.5 \times 10^{-8}(^{\circ}C)^{-2}$. This means that, to control the oscillator frequency to 1 ppm, the temperature must be held to within 3.65°C of T_0, or to control the frequency to 1 part in 10^8, the temperature must be stabilized within 0.365°C of T_0. The value of T_0 may be varied from below 0°C to above 100°C by changing the angle of the crystal cut from 35° to 38°. An even lower value of α may be obtained with quartz crystals whose Y-rotation angle is in the vicinity of -50.5°, i.e., very near the BT cut angle (Ref. 20).

The strain sensitivity of SSBW devices was measured for both ST cut quartz and 36° rotated Y-cut substrates. Table 3-2 is a summary of the results of these measurements. The coefficients $\gamma_1 - 1$ and γ_2 are equivalent to the Gage Factor (GF) used to describe ordinary resistance-type strain gages. For these gages, the GF typically has a value near 2. While the larger acoustic wave strain sensitivities are only about half as great as the GF of resistance-type gages, it should be borne in mind that the stability of the sensor and the degree of accuracy with which the sensor output can be measured weigh in favor of the frequency output acoustic wave devices. As a result, sensitivities of 1.0 or even less are considered very encouraging and deserving of further investigation. The results on 36° quartz are particularly attractive in view of the low temperature sensitivity. The good transverse strain sensitivity ($\gamma_2 \tilde{-} 1.0$) and the very small parallel sensitivity ($\gamma_1 - 1 \tilde{-} -0.05$) will make this configuration easy to design into a practical sensor. The ST cut SSBW devices have higher strain sensitivity than the 36° cut, but the high temperature coefficient for SSBW's on ST quartz (~ -31 ppm/°C) rules in favor of the 36° quartz.

Note, in Table 3-2, that the strain sensitivity of the 40 μm wavelength B38-L deice is only about half as great as that of the λ = 13 and 16 μm devices. The same dependence upon wavelength is also seen in the ST-cut devices. The angle beneath the surface at which the SSBW's are launched depends upon the wavelength with the shorter wavelength (higher frequency) waves being launched at a more shallow angle. Since the bending strains are highest at the surface and decrease linearly with depth into the substrate, it is believed that the larger strain sensitivity of the higher frequency waves is the result of these waves propagating through regions of greater strain. A quantitative understanding of this behavior will be sought in the follow-on program through a perturbation theory analysis of the strain sensitivity problem.

Because of its high strain sensitivity, very low temperature sensitivity, and tolerable fluid loading losses, a SSBW device on 36° quartz is considered a very attractive candidate for further development for sensor applications.

TABLE 3-1

DELAY LINE PARAMETERS

DL#	Pattern	Wavelength (microns)	Type of Electrodes	Aperture (WL)	Length (WL)	Transducer Spacing(WL)
1	FADEC2	40	double	51	120	40
2	SV-Q1-38-80	40	single	51	80	67
3	GAW XER-1	16	single	62	50	125
4	GAW XER-2	16	single	62	50	100
5	GAW XER-3	16	single	62	50	1
6	GAW XER-6	24	single	42	50	83
7	GAW XER-7	24	single	42	50	100
8	GAW XER-8	24	double	42	50	1
9	VSEXP2	24	double	50	50	87
10	AGW1A-1A	12	single	70	100	4
11	AGW1A-2B	16	single	70	100	4
12	AGW1A-4A	24	double	70	75	4

TABLE 3-2

STRAIN SENSITIVITY MEASUREMENTS
SSBW IN QUARTZ

Sample Number	Quartz Cut-Angle	Wavelength (microns)	Strain Sensitivity	
			Parallel $\gamma_1 - 1$	Transverse γ_2
B1	-42.75° (ST)	40	0.31	0.63
B20-2B	-42.75° (ST)	16	0.45	1.36
B38-L	-36°	40	--	0.62
B45-L	-36°	40	-0.05	0.50
B45-L	-36°	13	-0.07	0.96
B37b-B2	-36°	16	-0.04	1.02
B37b-C3	-36°	16	-0.05	0.97
B49-C3	-36°	16	-0.06	1.05

DEVICE CONFIGURATION
SSBW IN QUARTZ

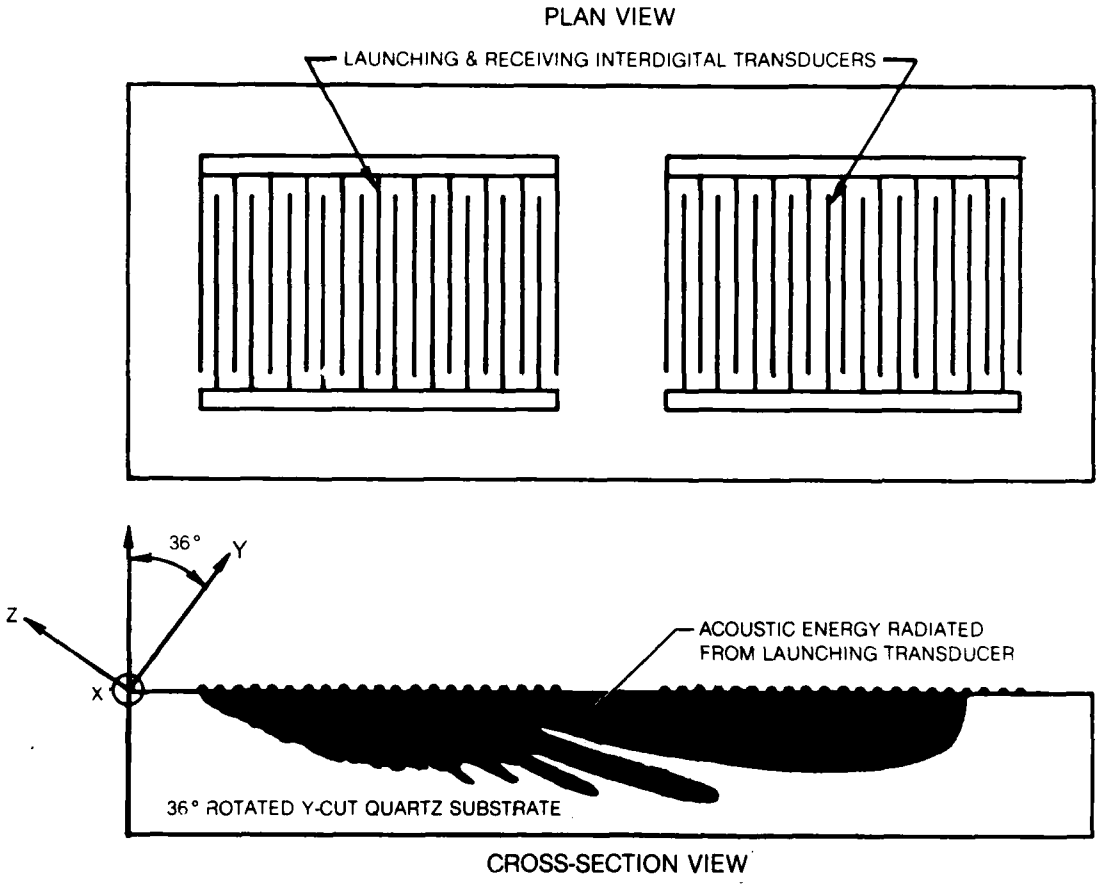

FIG. 3-2

INSERTION LOSS CHARACTERISTICS
SSBW IN QUARTZ

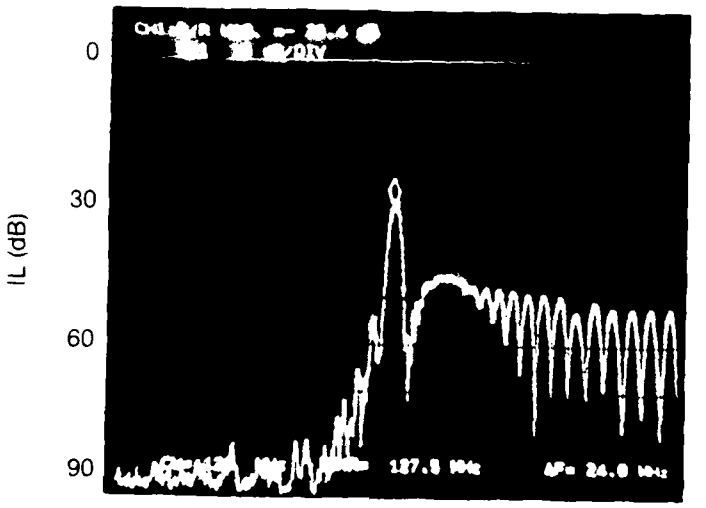

FUNDAMENTAL FREQUENCY

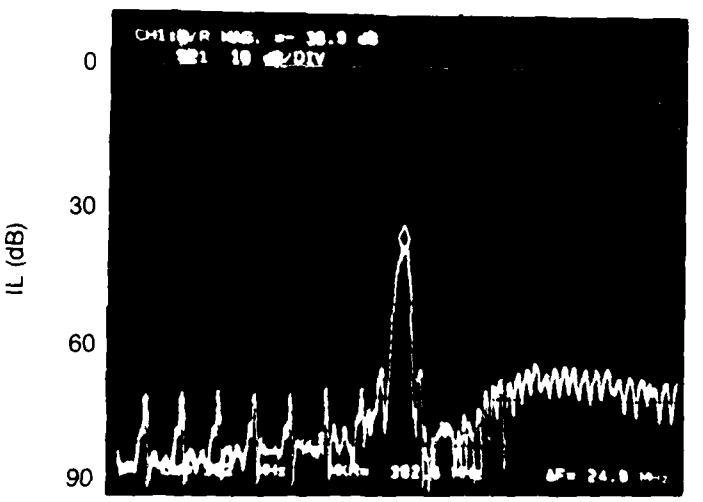

THIRD HARMONIC FREQUENCY

83-5-42-7

EFFECTS OF OIL IMMERSION SSBW IN 36°Y QUARTZ

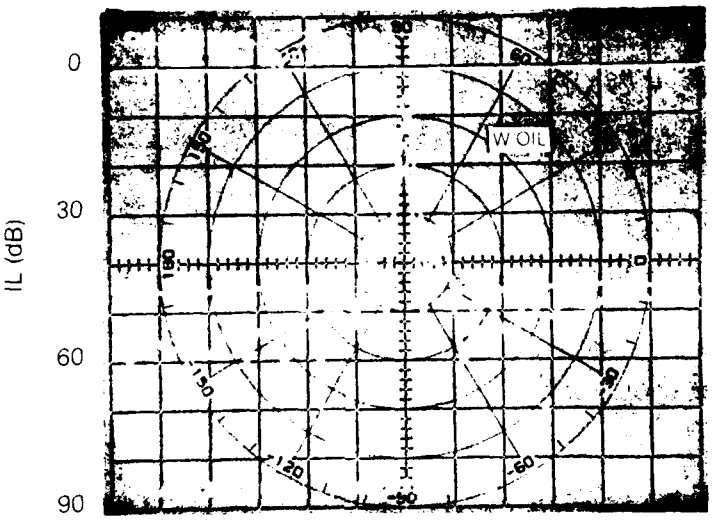

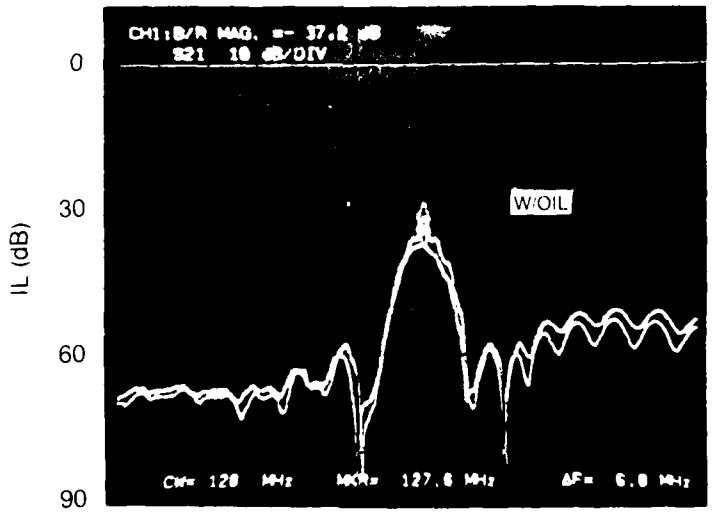

83-5-42-6

TEMPERATURE SENSITIVITY
SSBW IN 36°Y QUARTZ

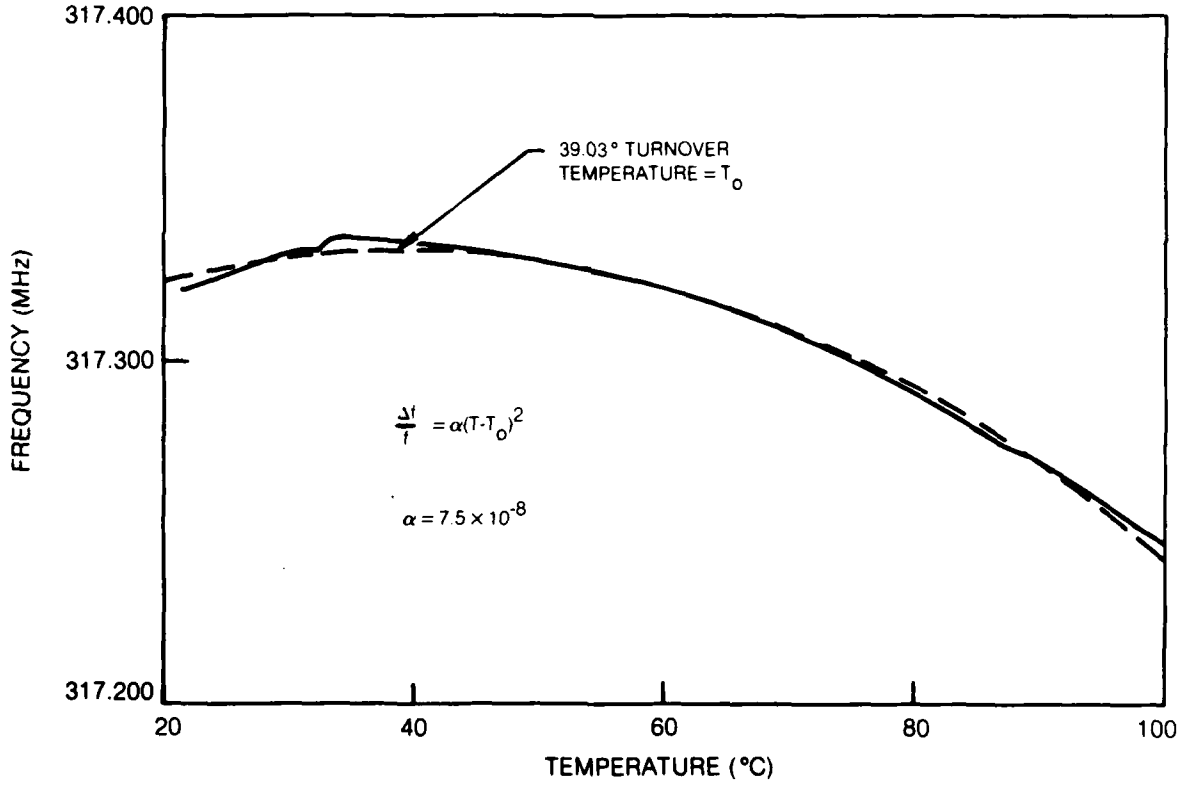

83-5-42-5

4.0 Acoustic Wave Modes in SiO_2/YX-$LiNbO_3$

The work performed on the SiO_2/YX-$LiNbO_3$ configuration during the course of this program is presented in a paper entitled "Surface and Interface Acoustic Waves in SiO_2/YX-$LiNbO_3$" which has been submitted to Applied Physics Letters. A preprint of this paper is included in this report as Appendix A. The investigation of the acoustic modes in this structure will be discussed further in the following.

Figure 4-1 shows the calculated dispersion curves and experimental data points for the allowed acoustic wave modes in the layered structure SiO_2/YX-$LiNbO_3$. In addition to the Rayleigh-type surface wave, two other modes are predicted and observed experimentally. One is a horizontally polarized surface shear wave (SH) and the other is an interface wave with displacement components localized at the SiO_2-$LiNbO_3$ interface. The interface wave was designated as a generalized Stonely wave (GSW). Figure 4-2 illustrates calculated particle displacement components for each of these two waves showing their distinct characteristics.

The effect of a massless shorting plane on the velocity dispersion is seen by comparing the curves for the open and shorted interface cases in Fig. 4-1. If the mass loading of a metal layer of finite thickness (1% λ) is included in the calculations, the result is a small reduction (< 5 m/s) in the velocity of both the SH and GSW modes and a small increase in the localization of the GSW wave at the metallized interface. Further increases in the metal thickness cause additional slowing of the waves but do not result in dramatic changes in either the velocities or displacement profiles.

It was anticipated that a mode such as the GSW mode could be obtained by placing a metal layer at the SiO_2-$LiNbO_3$ interface. The slower acoustic velocity of the metal layer would tend to "trap" the acoustic energy at the interface and produce the desired guided wave. Theoretically, the wave exists independent of the metal layer, and the addition of a finite thickness metal layer has little effect on the wave beyond that of a massless shorting plane. Figure 4-3 shows the calculated displacement profiles for the GSW wave at $h = \lambda$ for the open and shorted interface cases. As seen in the figure, the addition of a massless shorting plane leads to a reduction in velocity from 4043 m/s to 4035 m/s and displacement profiles that are more localized about the interface. The small reduction in velocity that is obtained by adding the shorting plane indicates that the acoustoelectric coupling to this mode is low. The analysis predicts a maximum value of $K^2 = 0.76\%$ at $h = 0.7\ \lambda$.

Experimentally, the GSW mode was obsered in the IL characteristics of all devices for which $h \geq 0.6\ \lambda$. Figure 4-4 shows the GSW and SH modes for two devices, one with $h = 0.60\ \lambda$ and Ti/Au/Ti metallization layer thickness $h_m = 0.011\ \lambda$, and the other with $h = 0.91\ \lambda$ and $h_m = 0.016\ \lambda$. As seen in Fig. 4-4, the two modes are quite close together in frequency and the IL of the GSW mode is between 6 and 10 dB greater than the SH mode. The coupling to the GSW mode was observed to decrease with increasing h/λ as seen by comparing the two samples in Fig. 4-4. Also shown in the figure is the effect of surface fluid loading on the two modes. In this case,the samples were not immersed in oil, but instead, a small drop of oil was placed on the SiO_2 surface in the area between

the IDTs. The result is only a small increase in the IL of the SH mode but a severe degradation of the GSW signal. As shown in Figs. 4-2 and 4-3, the vertical shear component of displacement is the dominant component of the GSW mode. The SV waves at the surface couple into P waves in the fluid, and, because the amplitude of the SV component at the surface is a significant fraction of the peak amplitude near the interface, substantial losses due to fluid loading are expected. As a result of this high sensitivity to surface fluids, temperature and strain sensitivity measurements on the GSW mode were not attempted.

In contrast to the GSW mode, the SH surface wave in $SiO_2/LiNbO_3$ was easy to excite and relatively insensitive to surface fluids. As a result, the SH mode was thoroughly characterized versus temperature and strain in order to assess the potential of this mode for sensor applications. Because SiO_2 and $LiNbO_3$ have temperature coefficients that are opposite in sign, it was expected that a zero value of TC could be found experimentally for the layered structure. Also, since the SH wave is a true surface wave with amplitudes decaying rapidly with depth below the surface, and the $LiNbO_3$ TC has a magnitude greater than the TC of SiO_2, it was anticipated that the zero TC value of h would be less than λ. Experimentally, samples with varying values of h/λ were processed and the temperature characteristics of the SH wave measured to locate the zero TC point. Having determined the value of h/λ that results in a zero first order TC, ($h/\lambda = 0.405$), strain sensitivity measurements were then performed on devices with h/λ near the zero TC value.

For values of $h/\lambda < 0.405$, the characteristic of the SH wave depends strongly upon the conditions (electrically open or electrically shorted) at the SiO_2-$LiNbO_3$ interface. As shown in Fig. 4-5, for $h = 0.4\ \lambda$, an open interface results in a lossy wave that radiates shear waves into the bulk. A shorting plane at the interface transforms the leaky wave into a bound mode. For $h > 0.405\ \lambda$, both open and shorted interfaces result in well defined SH surface waves as shown in Fig. 4-6 for $h = 0.5\ \lambda$. The experimental devices are best described by the open interface case in the region of the transducers. As a result the velocities determined by the frequency and wavelength (i.e., $v = f\lambda$) should conform to that predicted for the open interface. Refering to Fig. 4-1, that is seen to be the case except in the region around h .4λ where there is a significant spread in velocities. In all instances, the experimental velocity is less than the predicted value, presumably because of the inability to properly model the elastic properties of the SiO films. These films are known to be stressed (Ref. 3) and a complete model must also take that into account.

The results of temperature sensitivity measurements made on the SH mode in $SiO_2/YX\text{-}LiNbO_3$ are shown in Fig. 4-7. The zero first order TC at 20°C occurs at $h = 0.42\ \lambda$ and the second order coefficient at that point is 0.21 ppmm/°C^2. The TC is seen to be a rapidly varying function of h/λ in the vicinity of $h/\lambda = 0.42$ and is undoubtedly strongly influenced by the proximity to the $h = 0.405\lambda$ cut-off point. Controlling the processing of these devices in order to be able to consistently reproduce the zero TC SiO_2 thickness would appear to be a difficult task.

Strain sensitivity measurements made on the SH mode proved to be disappointing. The results of measurements on two devices with $h = 0.42\ \lambda$ gave values of $\gamma_1 - 1 = -0.21 \pm 0.03$ and $\gamma_2 = -0.31 \pm 0.10$. The maximum values of $\gamma_1 - 1$ and γ_2 obtained for all samples tested was $\gamma_1 - 1 = 0.52$ and $\gamma_2 = 0.53$ at $h/\lambda = 0.53$. As indicated by these two results, there was significant scatter in the strain sensitivity data. While the results obtained from a given sample were repeatable, values of γ_1 and γ_2 obtained from devices with similar h/λ ratios were not. It is conjectured that the measurements are strongly influenced by built-in film stresses which vary from device to device. The highest values obtained, however, are at best a factor of 2 below the level desired. This low stain sensitivity, together with the strong dependence of TC upon h/λ in the region of the TC = 0 value, make the SH mode an unlikely prospect for sensor application.

FIG. 4-1

PHASE VELOCITY VERSUS SiO_2 THICKNESS FOR SiO_2/YX-$LiNbO_3$

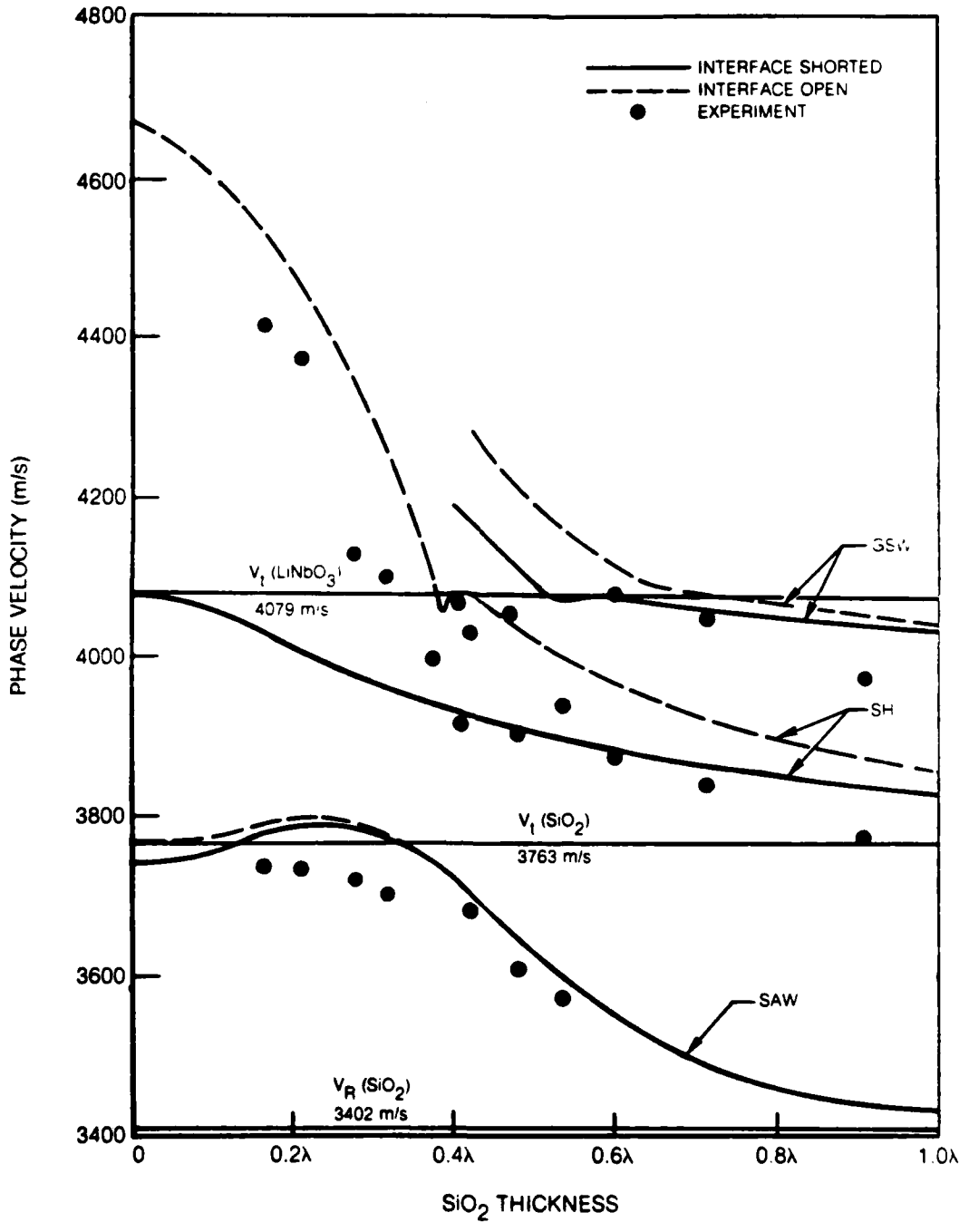

83-8-12-6

PARTICLE DISPLACEMENT COMPONENTS FOR SH-SURFACE AND GSW-INTERFACE WAVES

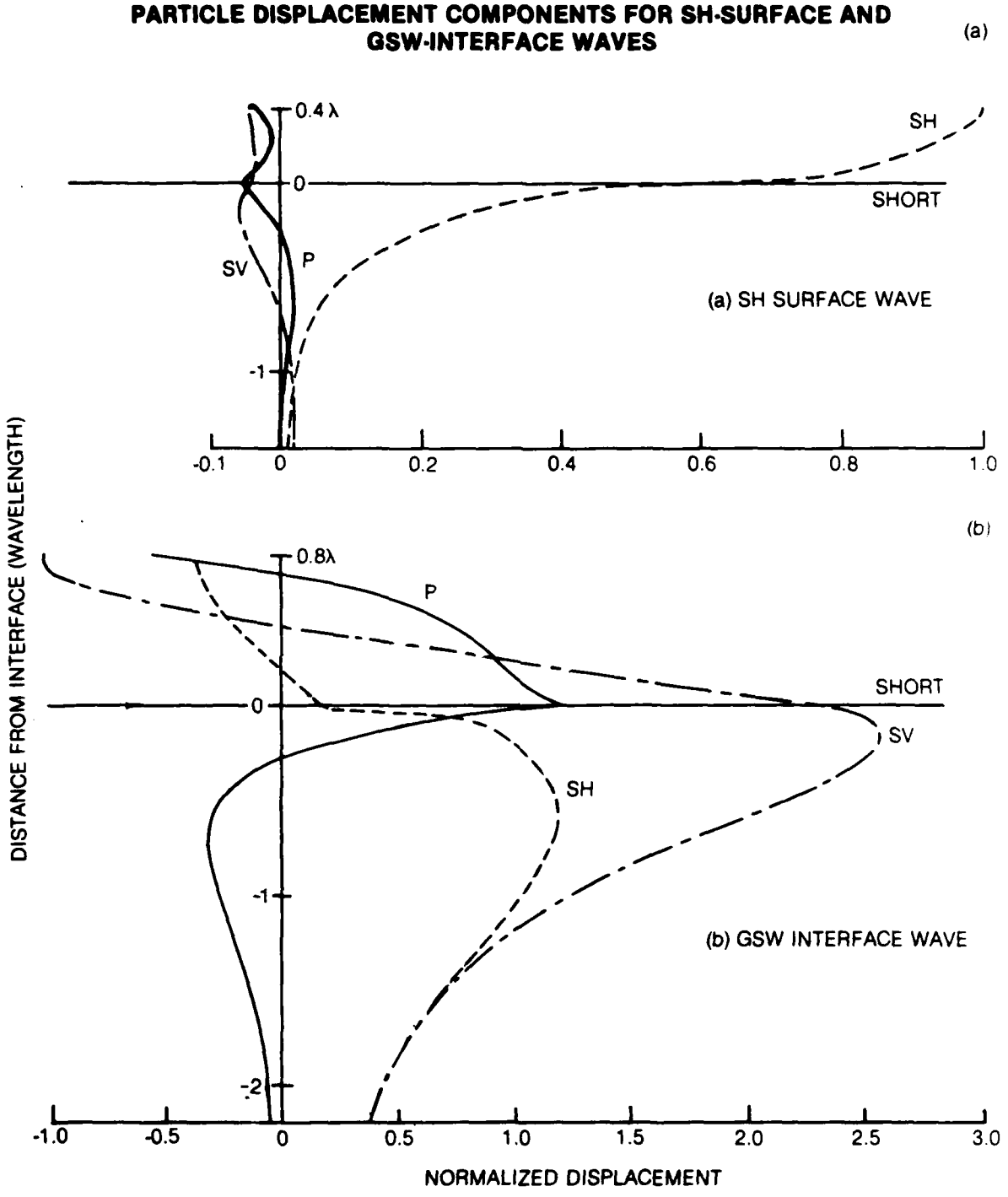

83-5-22-1

PARTICLE DISPLACEMENT COMPONENTS FOR GSW MODE IN 1.0λ SiO_2/YX-$LiNbO_3$

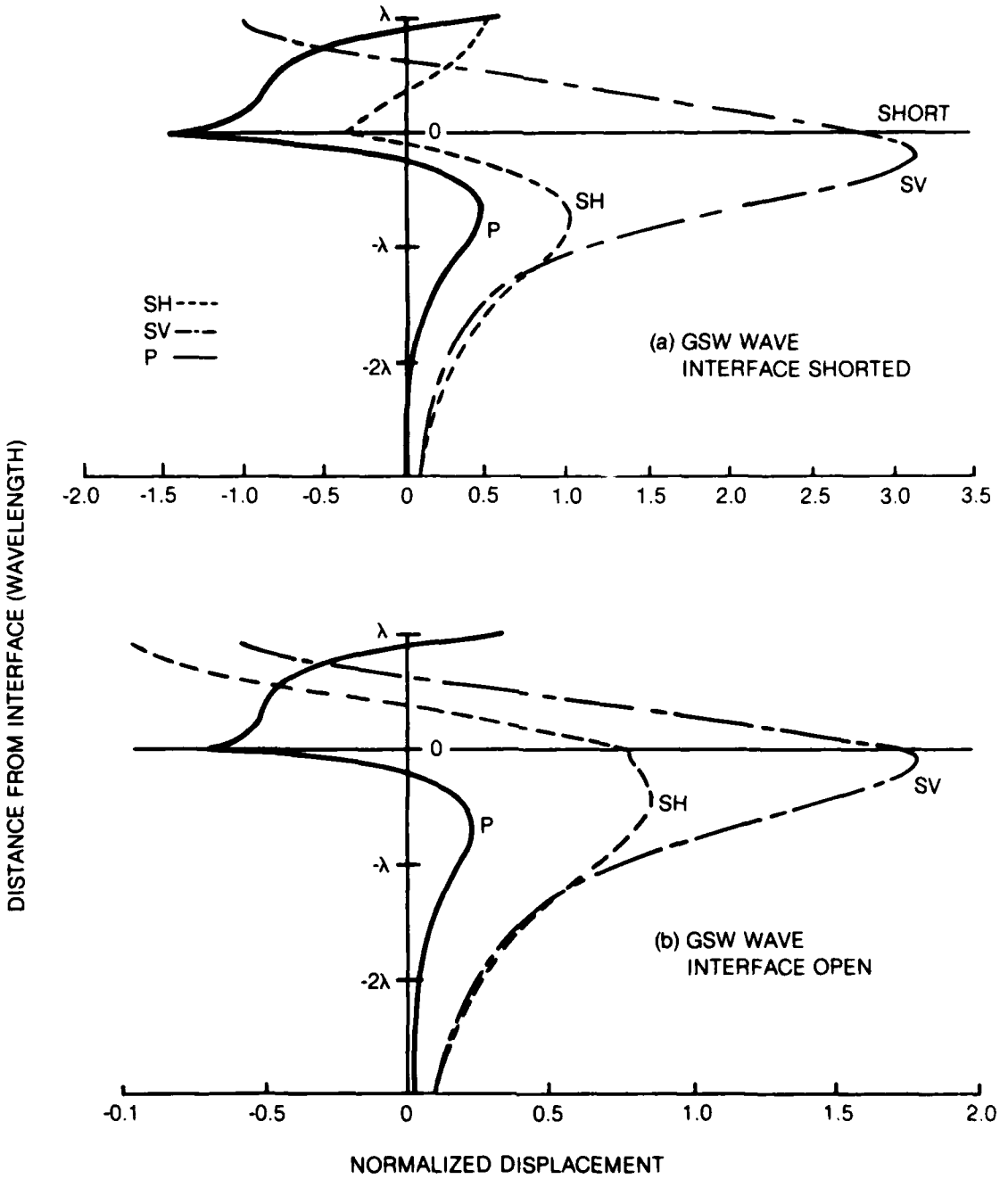

83-8-12-3

EFFECT OF SURFACE FLUID LOADING SiO_2/YX-$LiNbO_3$

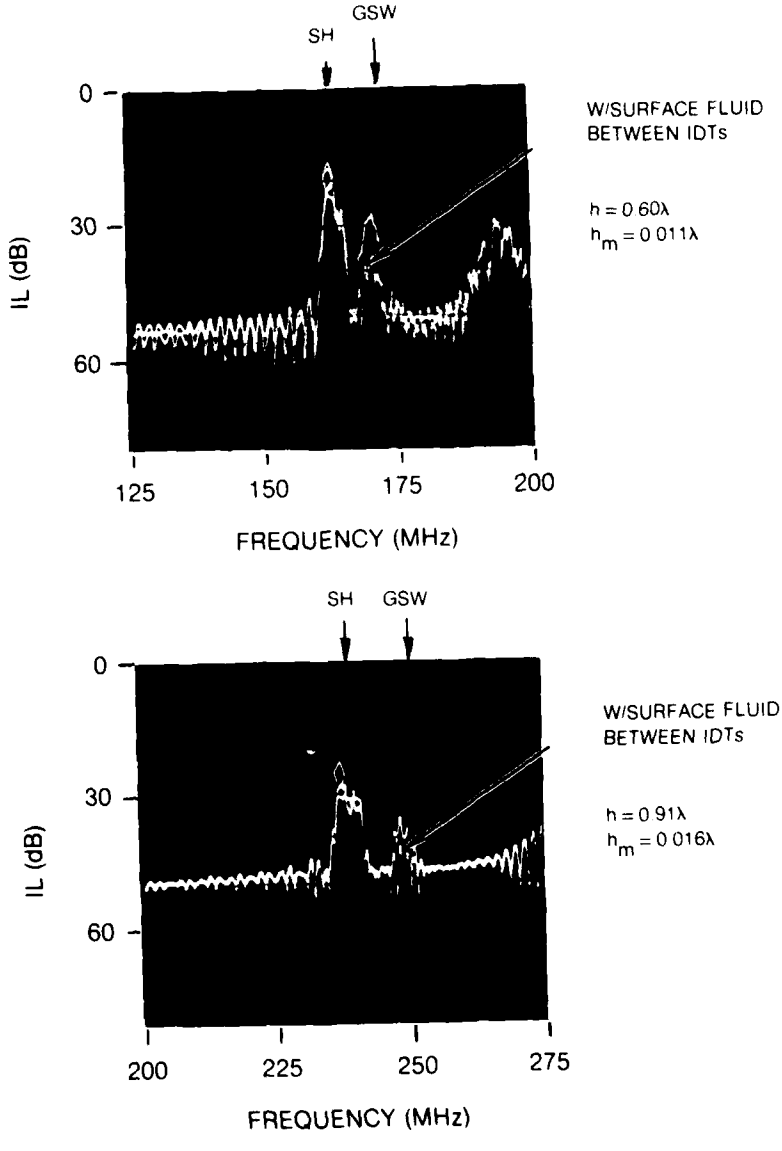

PARTICLE DISPLACEMENT COMPONENTS FOR SH WAVES IN 0.4λ SiO_2/YX-$LiNbO_3$

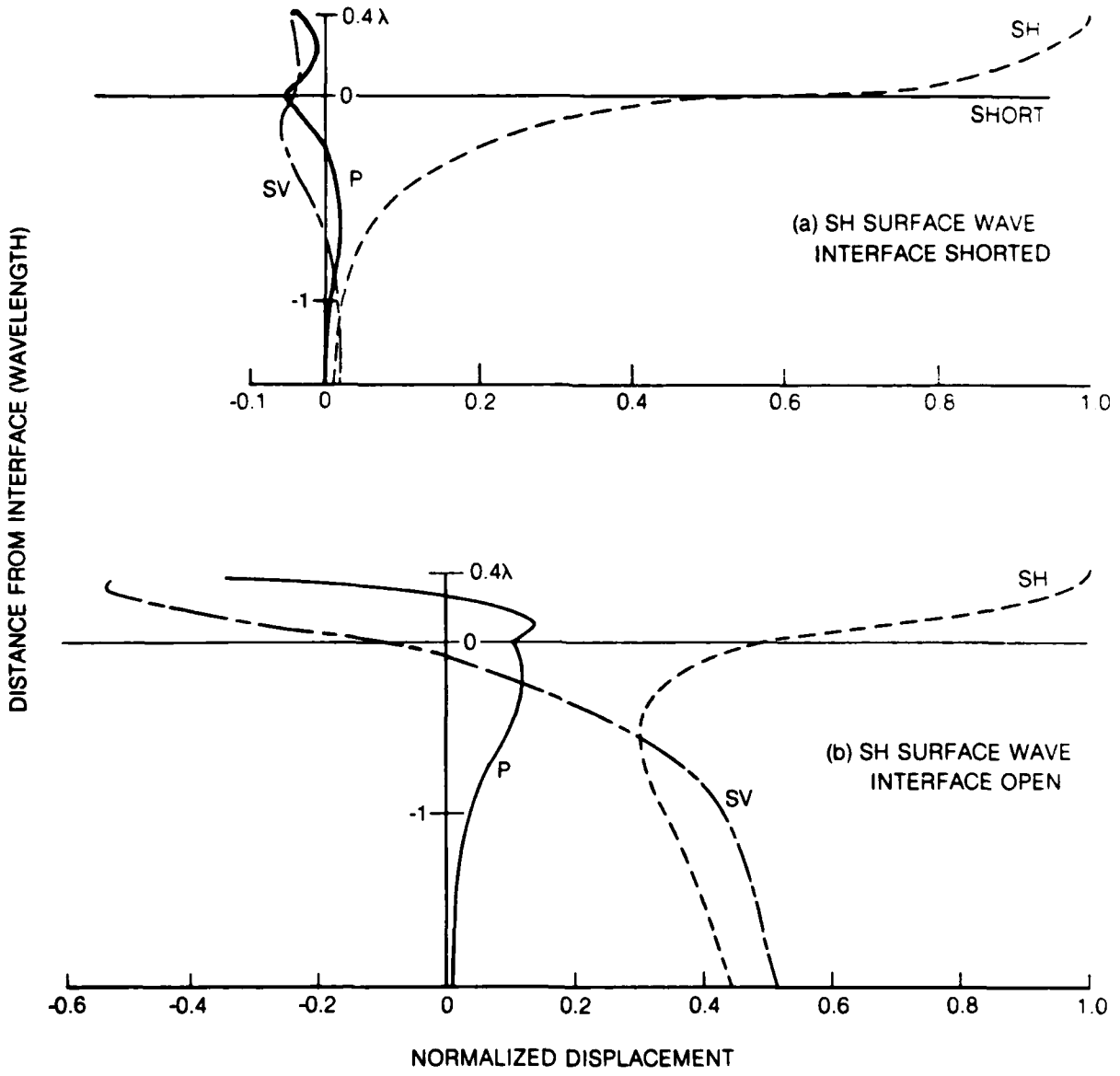

83-8-35-1

PARTICLE DISPLACEMENT COMPONENTS FOR SH WAVES IN 0.5λ SiO_2/YX·$LiNbO_3$

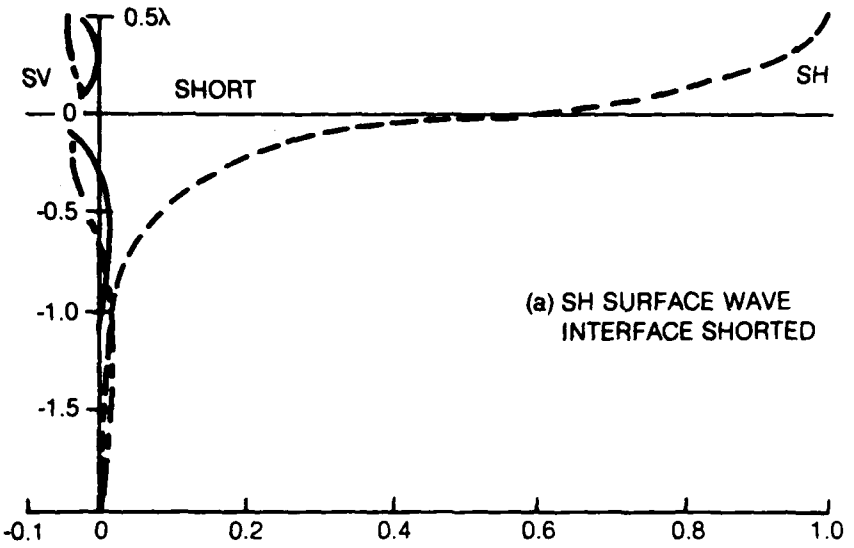

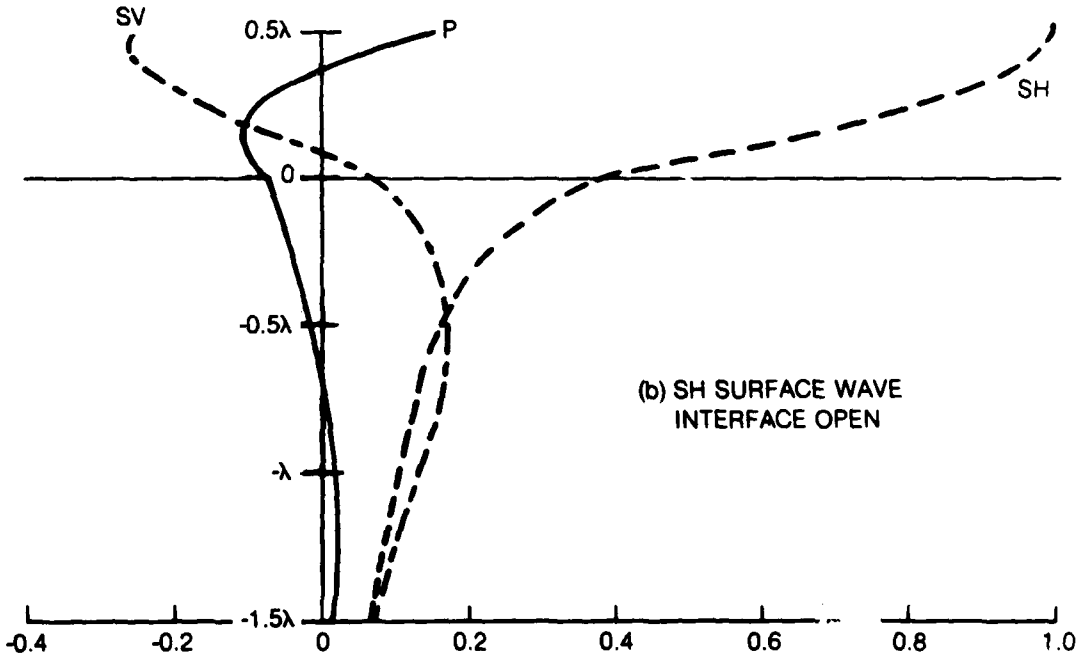

83-8-35-4

TEMPERATURE COEFFICIENT VERSUS SiO_2 THICKNESS FOR SH-SURFACE WAVE

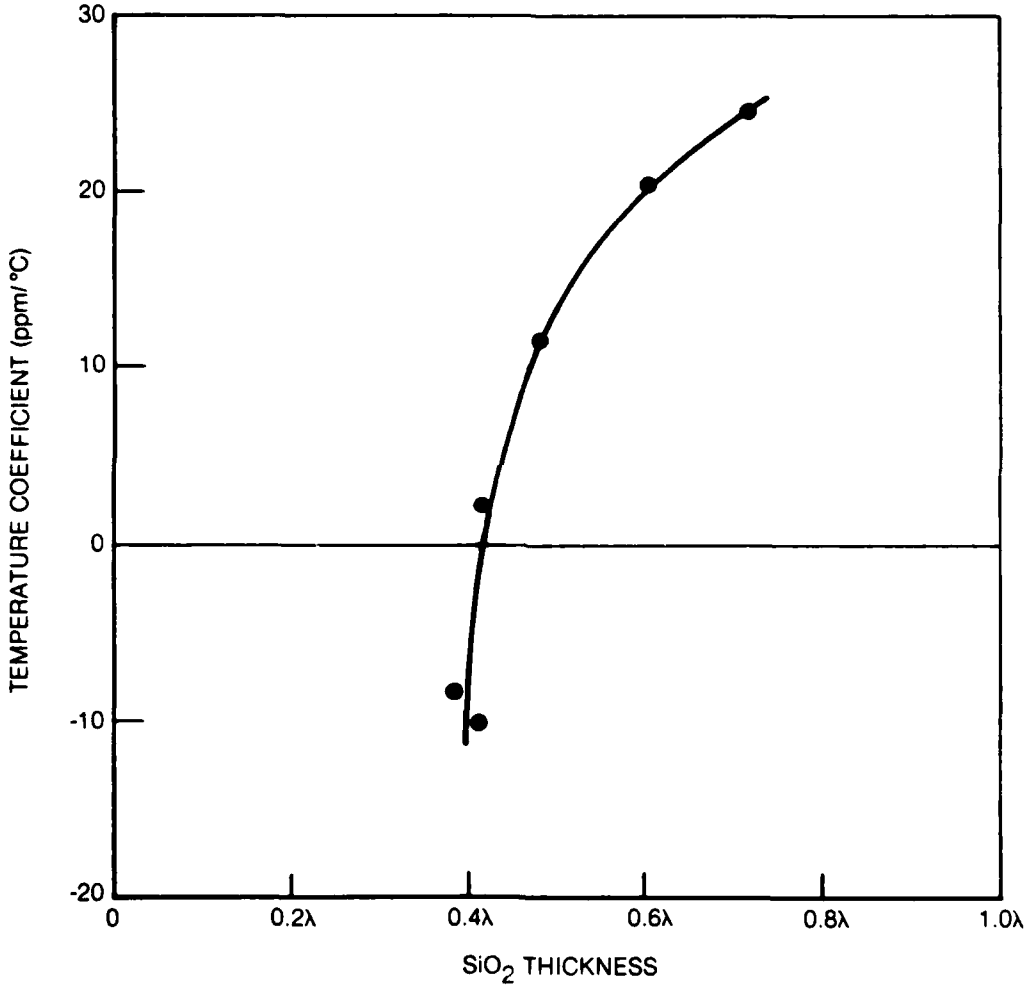

83-4-34-2

5.0 Acoustic Wave Modes in SiO_2/128° YX-$LiNbO_3$

Stoneley-like interface waves, or generalized Stoneley waves (GSW), have been reported in the layered structure SiO_2/126° YX $LiTaO_3$ (Ref. 2,3). Similarities between 126° YX-$LiTaO_3$ and 128° YX-$LiNbO_3$ suggested that localized interface waves might also exist in the $LiNbO_3$ layered structure. Because the acoustic energy is concentrated near the interface, the propagation of these waves should be insensitive to surface fluid loading. If these modes can be shown to possess the desired strain and temperature sensitivities, devices employing such modes could be developed into precision sensors. In this section, the results of a theoretical and experimental study of the acoustic wave modes in SiO_2/128° YX-$LiNbO_3$ are presented.

Propagation velocities, attenuations, and particle displacement profiles were calculated for silica films on 128° rotated Y-cut $LiNbO_3$. Three types of acoustic wave modes are supported by this structure: (1) a Rayleigh SAW, (2) a horizontally polarized shear surface wave (SH-SAW), and (3) two GSW's. The calculated dispersion curves, Fig. 5-1, show the effect of the SiO_2 film on the various modes. In general, the silica film loads the substrate and sharply reduces the propagation velocity. It also converts what is a predominantly Rayleigh-type leaky surface wave at zero SiO_2 thickness (V = 4007.6 m/s) into a nearly pure SH surface wave. Without the SiO_2 layer, the leaky-surface wave mode on 128° YX-$LiNbO_3$ has nearly the same velocity and characteristics as the Rayleigh surface wave(V = 3994.2 m/s). A thin film of SiO_2 converts the leaky mode into an unattenuated shear mode. The particle displacement profile of the SH-SAW mode for a $h = 1.1\lambda$ SiO_2 layer is plotted in Fig. 5-2. The SH mode was not strongly excited in any of the experimental devices and so was not further investigated.

Two additional modes appear in structures with thicker SiO_2 layers. They are the GSW modes whose properties are of prinicipal interest. These modes radiate energy into the substrate (see Fig. 5-3) until the propagation velocity is reduced by the SiO layer below the slow shear wave velocity in $LiNbO_3$ (V = 4079 m/s). As the SiO_2 thickness is increased, the velocity of both GSW modes approaches the shear velocity in SiO_2. Experimentally, the lower velocity, or Type I GSW, was easily excited. The insertion loss for this mode was as low as 10dB and less than 25dB for all samples examined. The Type II mode was strongly excited only with the thickest SiO_2 layers ($h > 1.2\lambda$).

The particle displacement profiles of the two GSW modes are shown in Figs. 5-4 to 5-7 for various SiO_2 layer thicknesses. The presence of a thin conducting layer at the SiO_2-$LiNbO_3$ interface reduces the propagation velocity of the GSW modes (see Fig. 5-1), but does not appreciably alter the mode profile. This can be seen by comparing Fig. 5-4a and Fig. 5-4b. As seen in Figs. 5-4 to 5-7, the peak amplitude of the Type I GSW does not occur at the interface but rather in the SiO_2 film. Also, the magnitude of the peak amplitude is only about twice as large as the amplitude at the free surface. The wave is not as tightly bound to the SiO_2-$LiNbO_3$ interface as anticipated, however, subsequent fluid loading experiments showed that the losses were not excessive. As h/λ increases within the range investigated, the Type II higher order GSW mode does become better localized at the interface. However, the magnitude of the peak amplitude is still only about twice the amplitude at the surface. Both of these modes might be better described as higher order surface waves rather than GSW's or interface waves.

Experiments were conducted to determine the SiO_2 thickness to wavelength ratio, h/λ, required to produce a zero first order TC for the Type I interface wave. Because the higher order interface wave was strongly excited only on samples with the thickest SiO_2 layers, its temperature properties were not investigated. Five samples with h/λ values of 0.76, 1.04, 1.16, 1.31, and 1.75 were tested versus temperature. Figure 5-8 shows the results of these experiments. A zero value of the first order TC at 20°C can be obtained at $h = 1.24\lambda$. The sample with $h = 1.16\lambda$ had a zero first order TC at -12.7°C, and the sample with $h = 1.31\lambda$ had a zero first order TC at 50.0°C. Figure 5-9 shows a frequency versus temperature plot and the parabolic fit to the data for the $h = 1.31\lambda$ sample. The second order TC for this device was 0.044 ppm/°C^2 at 50.0°C giving this device the lowest temperature sensitivity of all of the devices examined during the course of this program, including the SSBW devices on 36°Y quartz. The Type I GSW can, therefore, be temperature compensated and it remained to determine the strain sensitivity and the effects of fluid loading to fully assess the potential of this mode for sensor applications.

Experiments to determine the effects of surface fluid loading were also encouraging. Figure 5-10 shows the insertion loss versus frequency characteristics for the sample with $h = 1.04\lambda$. The Rayleigh-SAW and the Type I interface wave stand out clearly against a clean background signal. The SH-SAW is seen to be very weak at this value of h/λ, and the Type II interface wave is not observed at all. Figure 5-11 shows the effect of coating the entire device with a silicone oil. The Rayleigh-SAW is totally absorbed while the Type I wave suffers only a 10dB increase in attenuation. For values of h/λ closest to the zero TC value, i.e. $h = 1.16\lambda$ and $h = 1.31\lambda$, fluid loading losses were in the 7 to 10 dB range (see Fig. 5-12). Since the insertion losses without surface fluids were typically 15dB for these devices, the total losses were 22 to 25dB, well within the acceptable range. It should be noted that these devices have not been optimized and, therefore, the overall losses, including fluid loading, can undoubtedly be reduced to below 20dB. Figure 5-13 shows the insertion loss and effects of fluid loading on a sample with $h = 1.75\lambda$. This is the only sample in which the coupling to the Type II GSW was large enough to produce a clean signal. Fluid loading losses for the Type I wave are much greater than for the Type II wave at this value of h/λ. This follows from the displacement profiles of Fig. 5-7 which show the Type II wave to be better confined to the interface.

Measurements to determine the strain sensitivity of the Type I interface wave were performed on devices with $h = 0.76\lambda$, 1.16λ, and 1.31λ. Two devices with $h = 0.76\lambda$ were examined first with encouraging results. Values of $\gamma_1 - 1 = -0.66 \pm 0.02$ and $\gamma_2 = 0.68 \pm 0.17$ were obtained. These values are equivalent to the gage factor of ordinary strain gages. Since the acoustic devices can be used in pairs or groups of four to take advantage of the differing parallel and perpendicular strain sensitivities and, at the same time, cancelling deleterious temperature effects, the above sensitivities obtained with the $h = 0.76\lambda$ device are considered large enough to be useful in practical devices. It was hoped that the strain sensitivities for devices near the zero TC point would be at least as large. This does not seem to be the case however. Measurements to determine the strain sensitivity of $h = 1.16\lambda$ and 1.31λ devices showed first, that, with the thicker SiO_2 layers, the strain sensitivities were low, and second, that stresses in the SiO_2 films were strongly influencing the results. The frequency versus strain data for these devices all exhibited nonlinearities, making accurate determination of the

strain sensitivities impossible. It is estimated, from the data available, that the strain sensitivities, $\gamma_1 - 1$ and γ_2, for these devices are less than 0.2. These values are probably too low for practical sensor development, however, the effects of film stresses upon the apparent strain sensitivities is unknown. Since it is known that deposition of SiO_2 films onto $LiTaO_2$ by plasma-CVD rather than rf sputtering results in greatly improved interface wave propagation characteristics (Ref. 3), and it is probable that this is the results of reduced film stresses, it would be advisable to fabricate and test $LiNbO_3$ devices made with plasma-CVD. The Type I interface wave has excellent temperature properties and acceptable fluid loading losses, and an accurate picture of the strain sensitivities should be obtained before ruling out this configuration.

FIG. 5-1

PHASE VELOCITY VS SiO_2 THICKNESS FOR SiO_2/128° YX-$LiNbO_3$

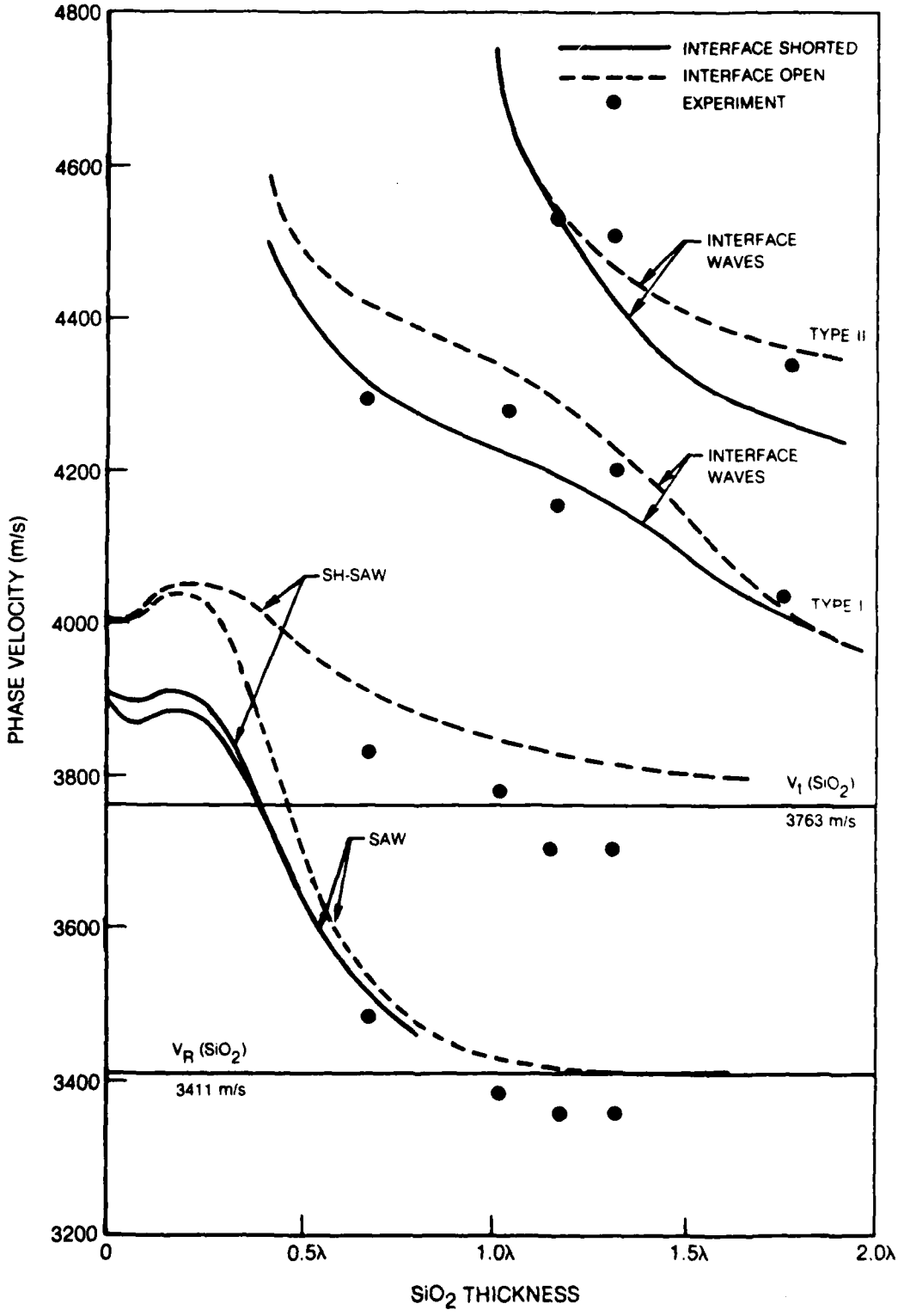

83-8-12-5

PARTICLE DISPLACEMENT COMPONENTS FOR SH-SURFACE WAVE IN 1.1λ SiO_2/128°YX-$LiNbO_3$

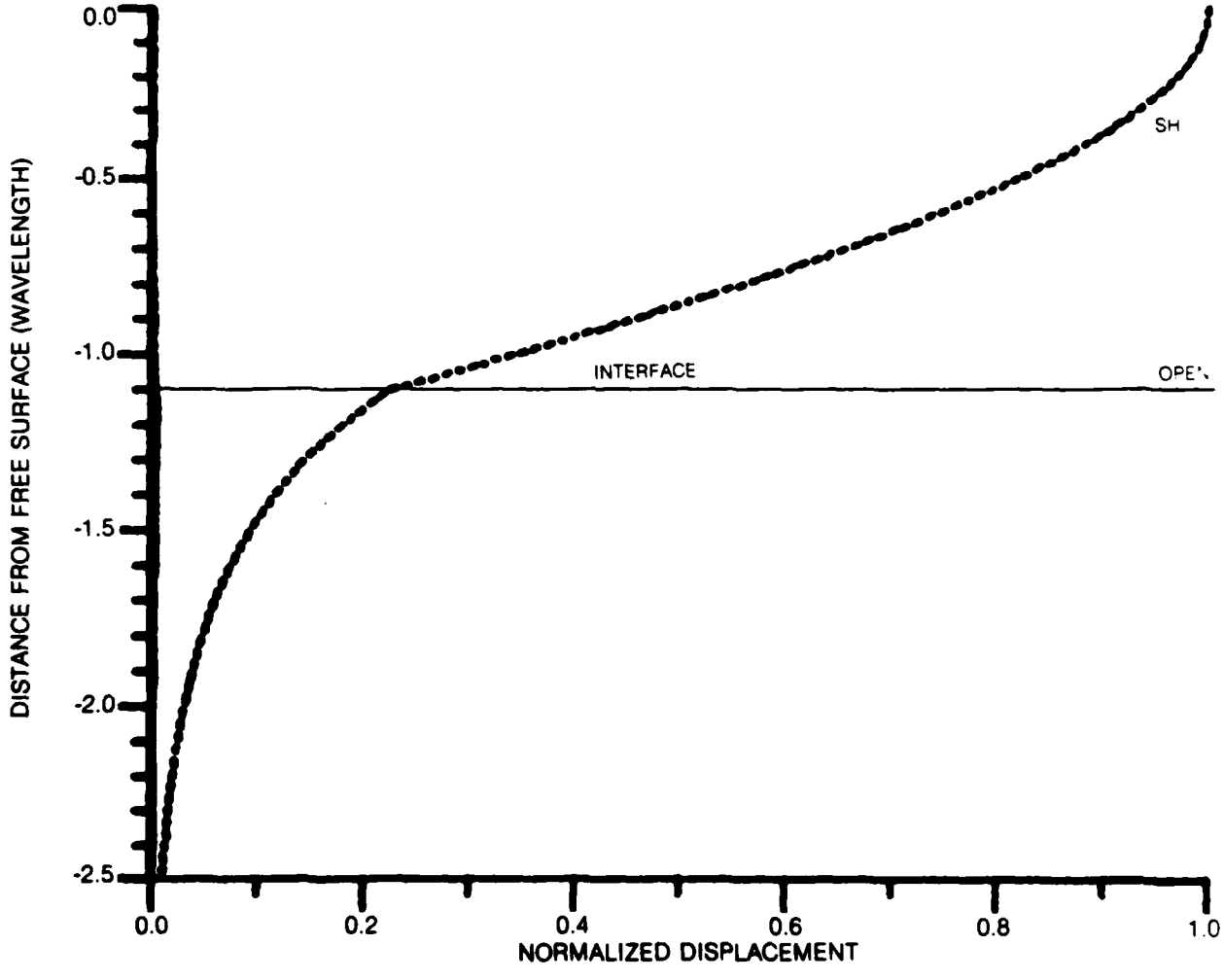

83-8-101-12

GSW MODE ATTENUATION VS LAYER THICKNESS IN SiO_2/128°YX-$LiNbO_3$

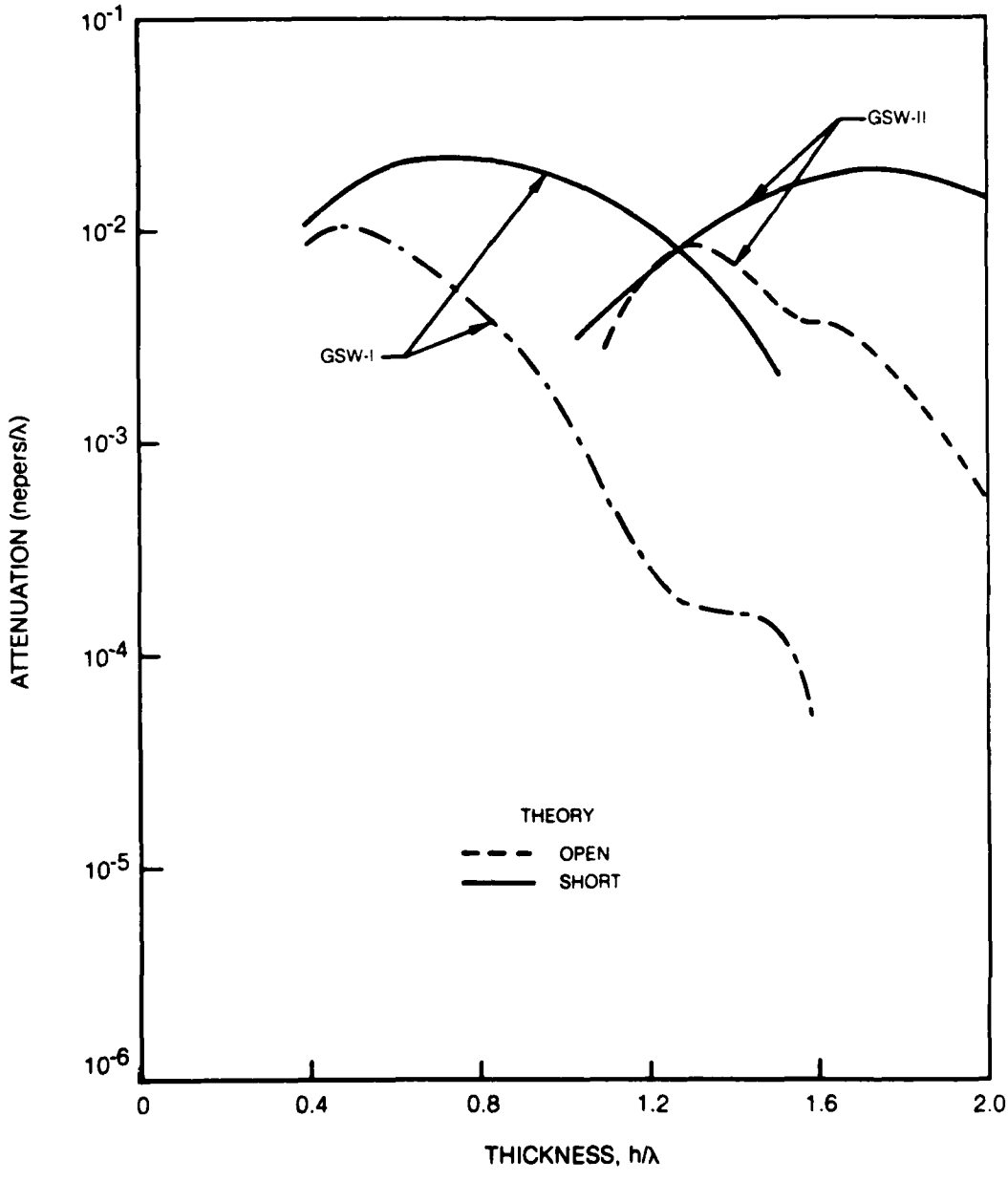

83-8-101-11

FIG. 5-4

PARTICLE DISPLACEMENTS FOR GSW TYPE-I MODE IN 1.1λ SiO_2/128° YX-$LiNbO_3$

a)GSW TYPE-I MODE INTERFACE SHORTED

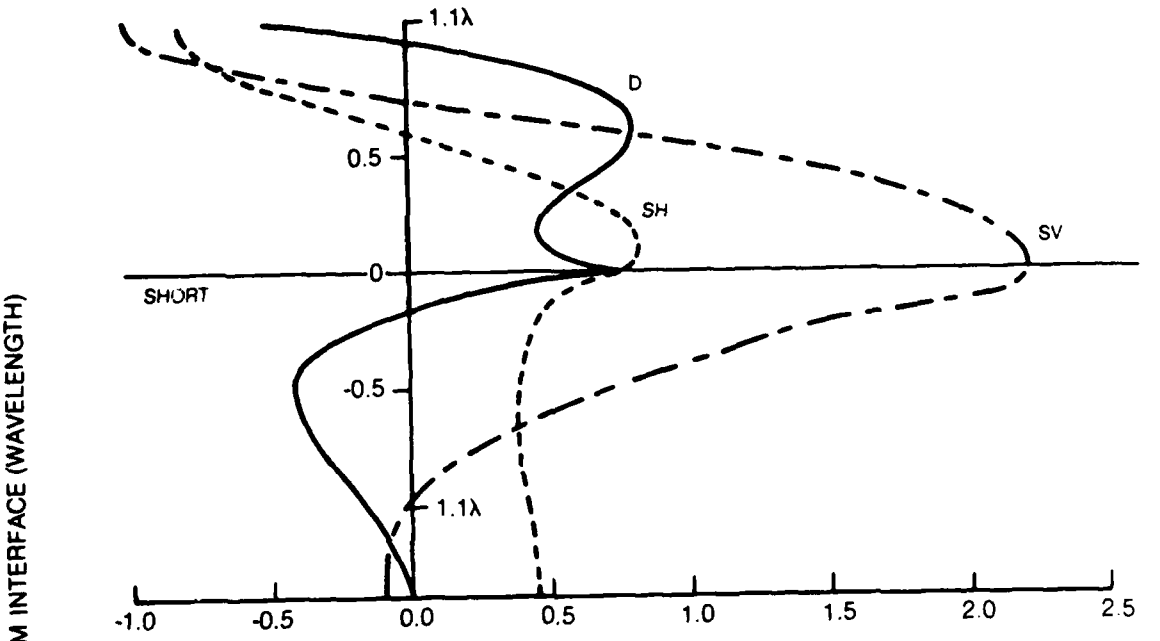

b)GSW TYPE-I MODE INTERFACE OPEN

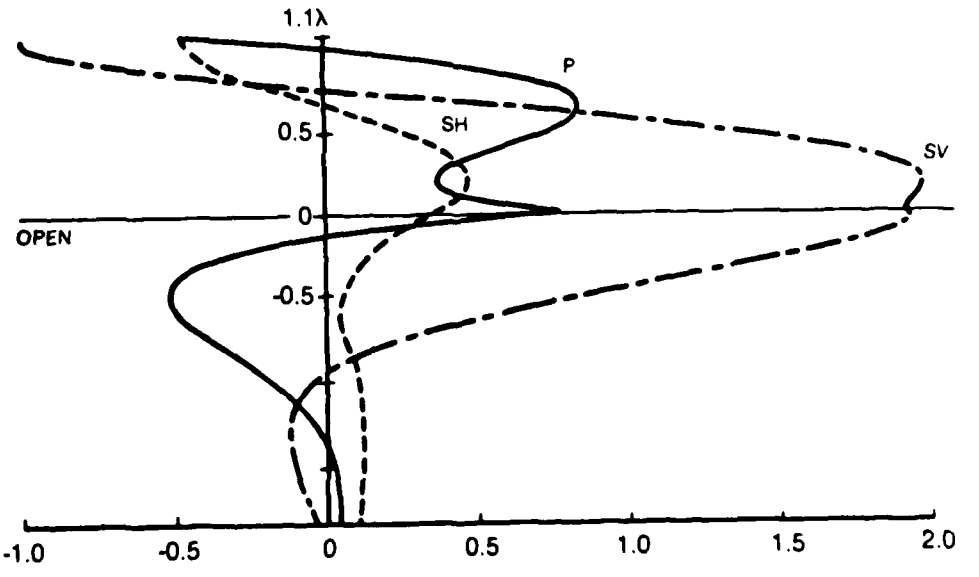

DISTANCE FROM INTERFACE (WAVELENGTH)

NORMALIZED DISPLACEMENTS

83-8-101-14

PARTICLE DISPLACEMENTS FOR GSW MODES IN 1.3λ SiO_2/128°YX-$LiNbO_3$

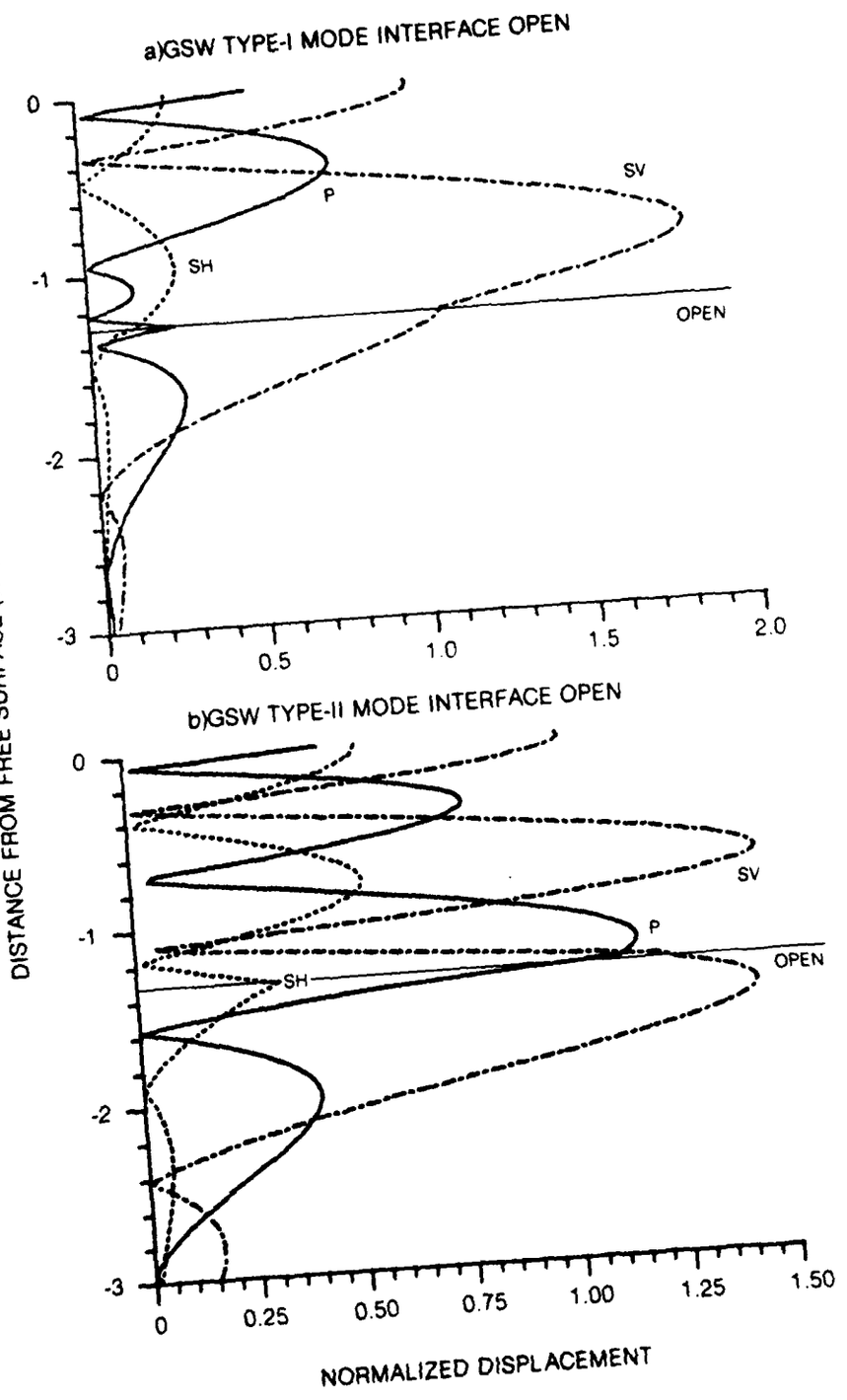

83-8-101-15

FIG. 5-6

PARTICLE DISPLACEMENTS FOR GSW MODES IN SiO_2/128°YX-$LiNbO_3$

a)GSW TYPE-I MODE INTERFACE AT 1.45λ

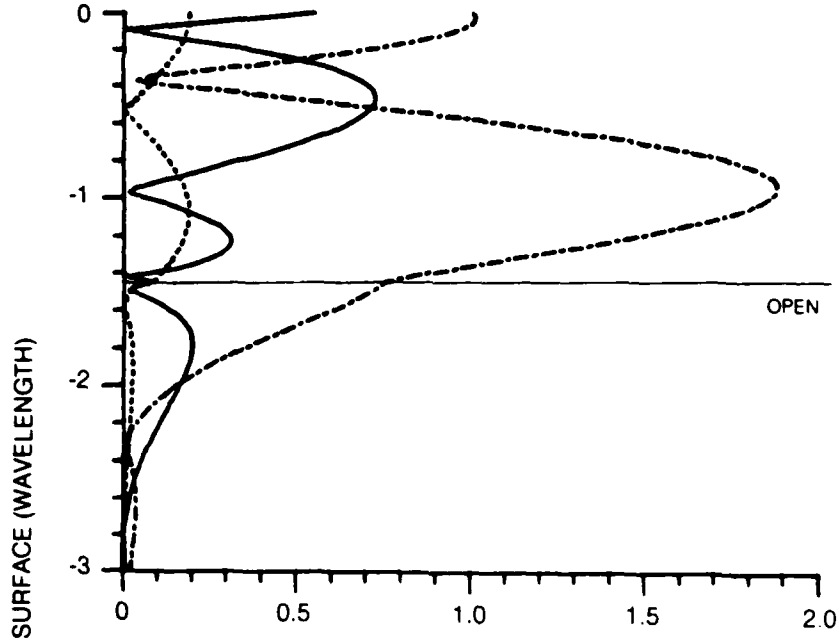

b)GSW TYPE-II MODE INTERFACE AT 1.55λ

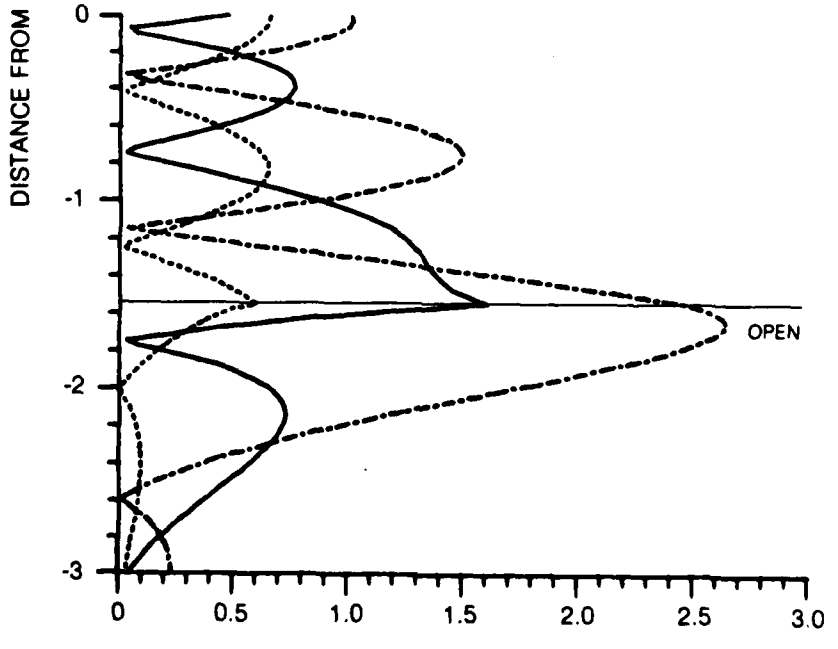

DISTANCE FROM FREE SURFACE (WAVELENGTH)

NORMALIZED DISPLACEMENT

83-8-101-16

PARTICLE DISPLACEMENTS FOR GSW MODES IN 1.75λ SiO_2/128° YX-$LiNbO_3$

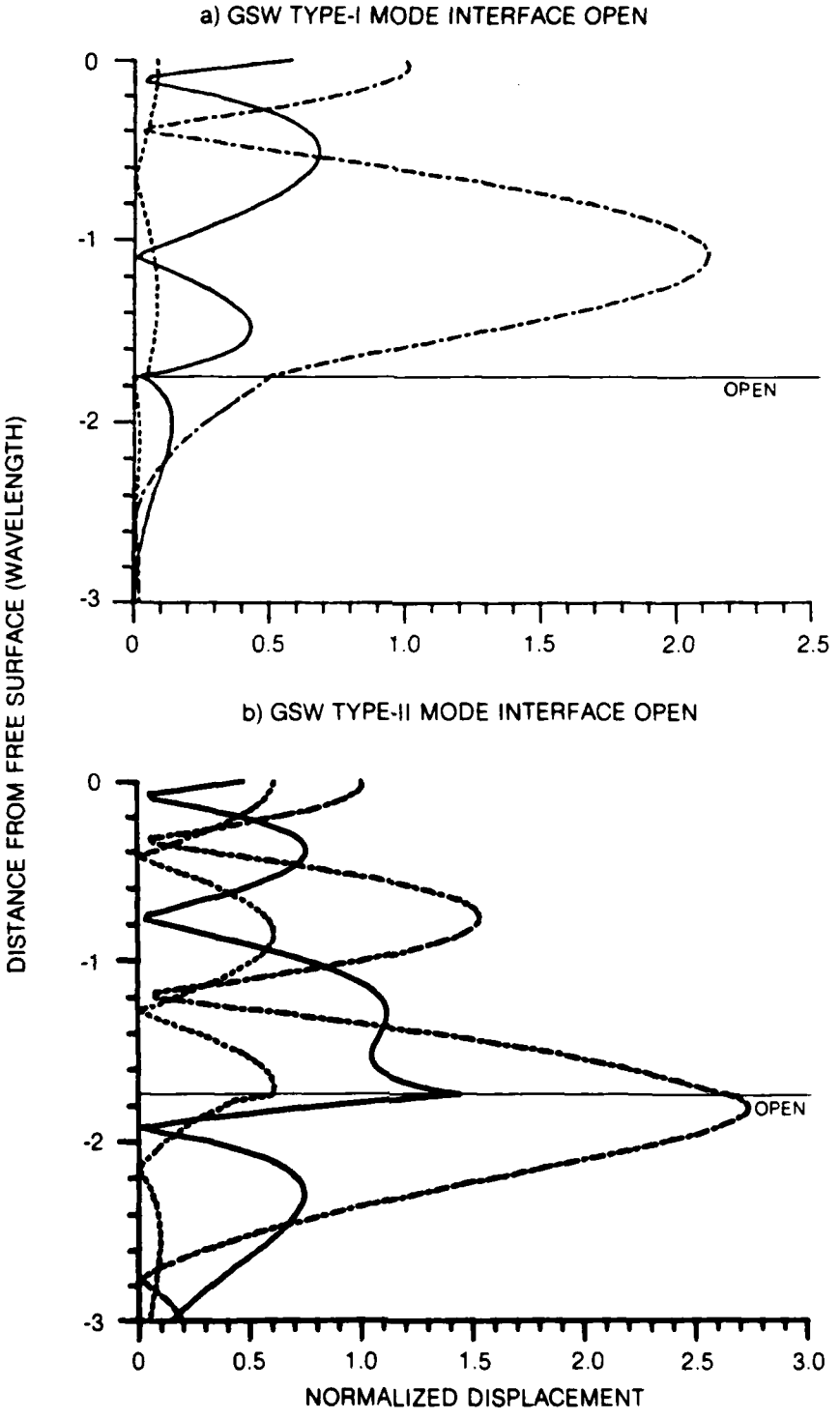

83-8-101-13

FIG. 5-8

SiO_2/128°YX-$LiNbO_3$ GSW WAVE TEMPERATURE COMPENSATION

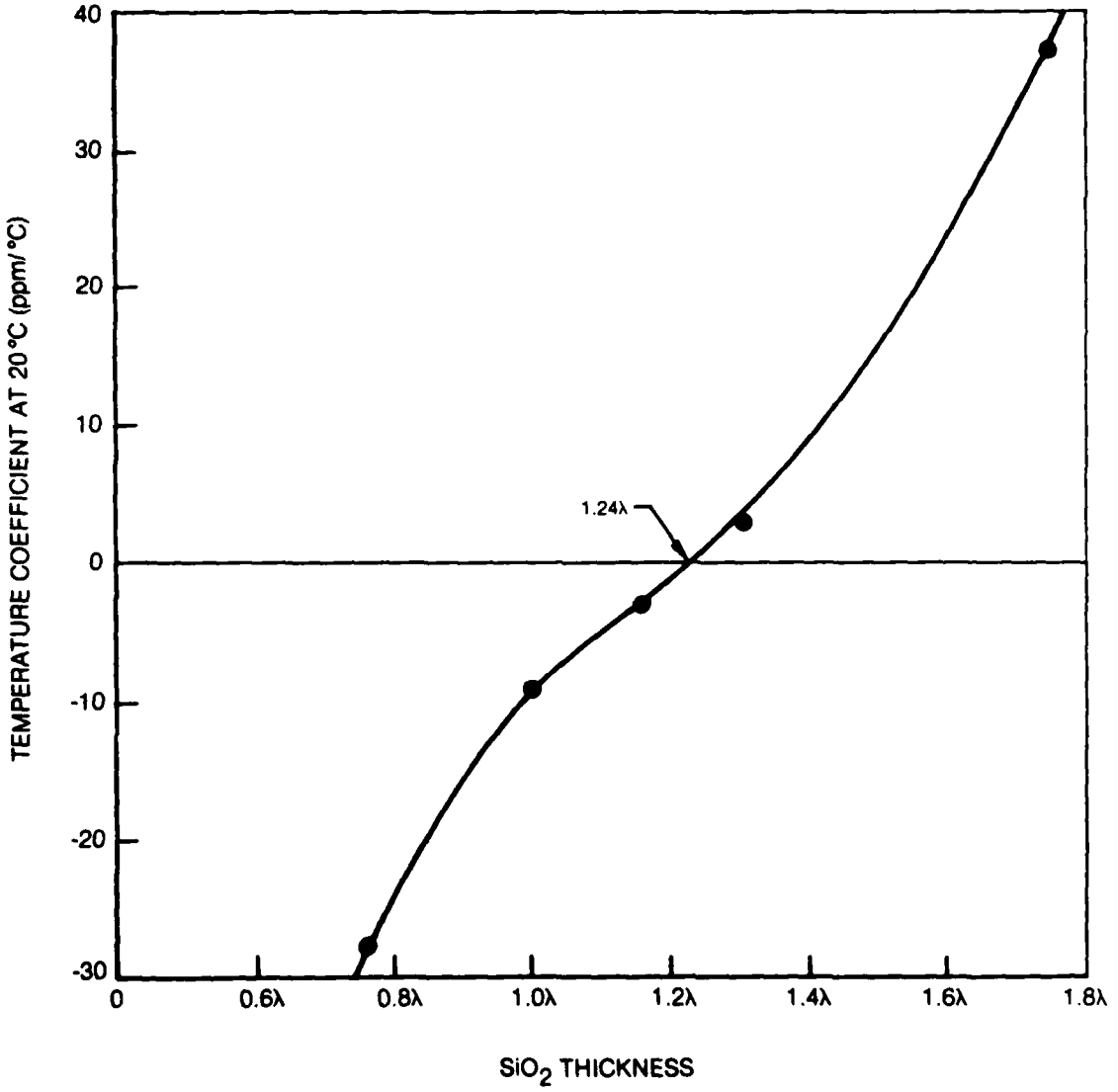

83-8-12-1

FIG. 5-9

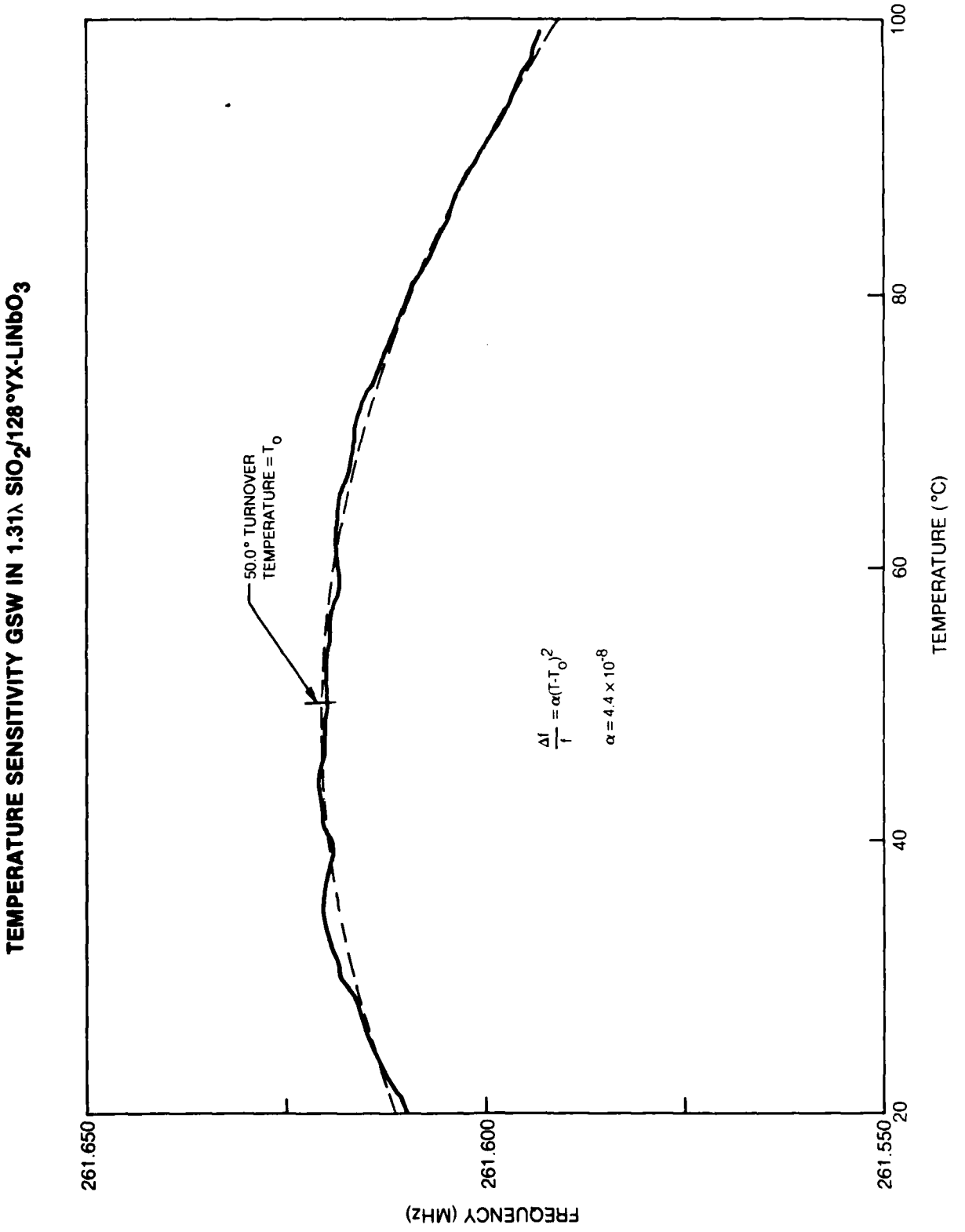
TEMPERATURE SENSITIVITY GSW IN 1.31λ SiO2/128°YX-LINbO3
50.0° TURNOVER TEMPERATURE = T0
Δf/f = α(T-T0)2
α = 4.4 x 10-8
FREQUENCY (MHz)
261.650
261.600
261.550
20
40
60
80
100
TEMPERATURE (°C)
83-8-12-7

FIG. 5-10

INSERTION LOSS CHARACTERISTICS
GSW IN 1.04λ SiO_2/128°YX-$LiNbO_3$

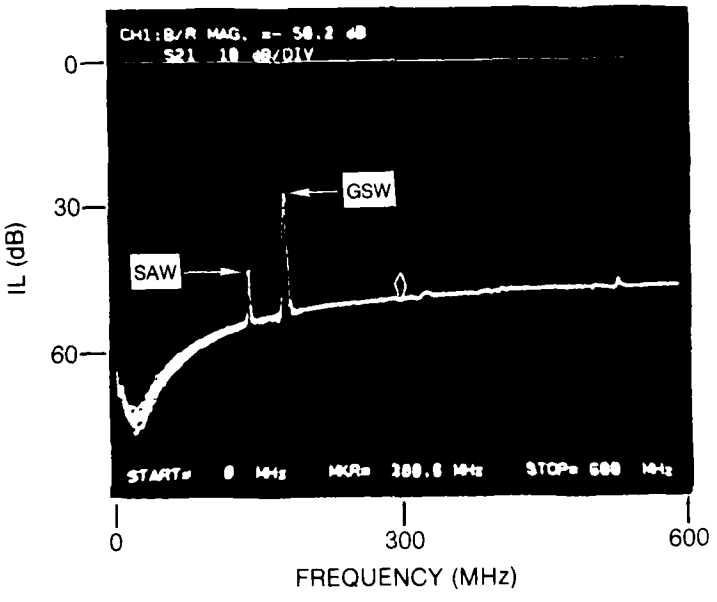

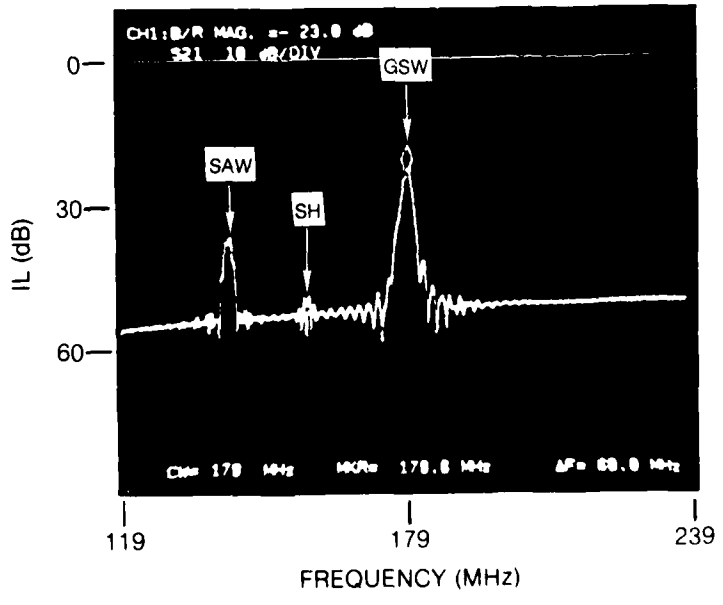

83-8-12-8

EFFECT OF OIL IMMERSION
GSW IN 1.04λ SiO_2/128°Y $LiNbO_3$

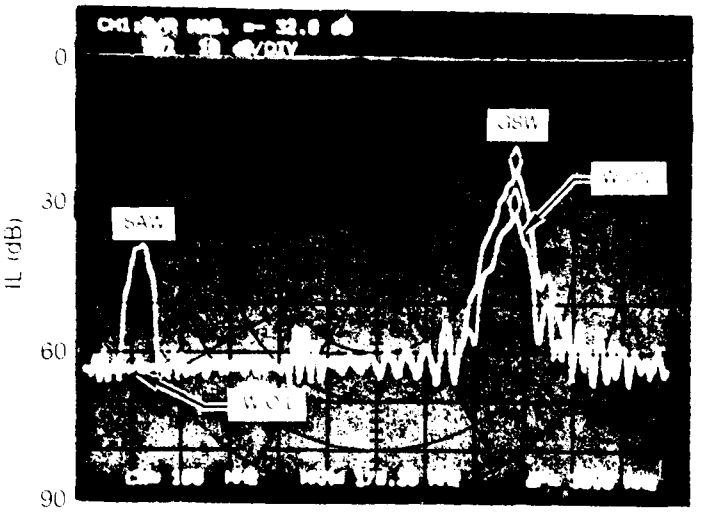

EFFECTS OF OIL IMMERSION

1.16λ SiO_2 128°Y-X $LiNbO_3$

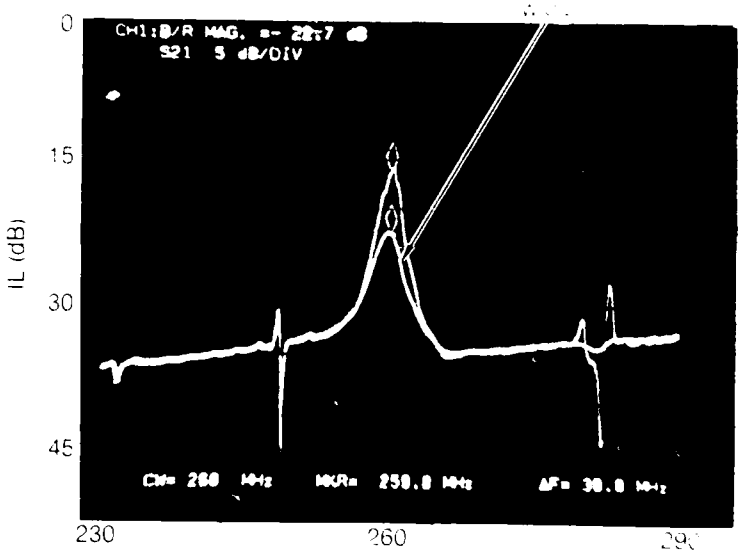

EFFECTS OF OIL IMMERSION
GSW IN 1.75λ SiO_2/128°YX-$LiNbO_3$

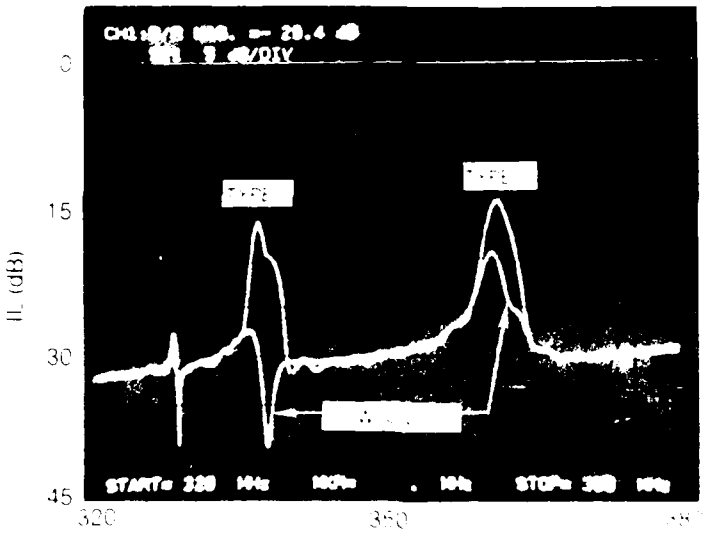

6.0 Summary and Recommendations for Continued Development

At the outset of the program very little was known of the acoustic properties or strain sensitivity of subsurface acoustic wave modes, or of the substrate configurations which would support them. The principal objective of the investigation was to identify promising SSAW modes relevant to sensor development. Strain sensitivity, temperature sensitivity, coupling efficiency, propagation losses and sensitivity to fluids placed on the surface were among the important characteristics to be determined. Materials and acoustic modes were sought that give rise to high strain sensitivity and low temperature sensitivity with minimum perturbation by surface fluid loading of the type required for vibration damping of a cantilever beam acceleration sensor.

The program successfully achieved its objectives through the careful theoretical and experimental examination of the acoustic modes supported by several candidate configurations. Table 6-1 summarizes the principal strain and temperature sensitivity results. Of the several substrate configurations and modes studied, the SSBW in 36° Y-cut quartz was found to possess the desired characteristics meriting further development as tabulated in Table 6-2. The configuration has good strain sensitivity, very low temperature sensitivity, and low sensitivity to surface fluid loading. Because a film overlay is not required, this SSBW device is more readily processed and the problems inherent to layered structures, i.e. film adherence, film stresses, thermal expansion matching problems, etc., are avoided.

The Type I GSW in SiO_2/128°YX-$LiNbO_3$ was thought to have potential at one point in the program, however, difficulties associated with stresses in the SiO_2 films make this configuration appear less attractive at this time. This mode has low sensitivity to surface fluid loading and actually has a lower temperature sensitivity than the SSBW on 36° Y-cut quartz. Unfortunately, the strain sensitivity also appears to be low, but has not been accurately established due to problems associated with stresses in the SiO_2 films. Methods of SiO_2 deposition that result in films with lower stress levels need to be investigated before a final decision can be made on this configuration.

Several other configurations which initially appeared promising were also eliminated. Configurations utilizing $LiTaO_3$ substrates were eliminated because of the susceptibility of the material to fracture. A layered SiO_2/Y-cut $LiNbO_3$ configuration was studied and discovered to support a shear horizontal (SH) polarized surface wave. Although a temperature compensating SiO_2 thickness was found, negligible strain sensitivity was measured. This novel result may prove important for stable oscillator applications requiring minimal sensitivity to mounting strains, but is rejected for the present sensor application.

The configuration shown in Fig. 1-1C considered the use of a intermediate thin film layer which would promote acoustic wave guiding near the interface. This configuration proved to have no advantage over the approaches shown in Cases A and B and was more complex to fabricate.

Another major accomplishment performed in parallel with this effort under a corporate sponsored program was the development and refinement of UTRC's theoretical modeling capabilities. Using the UTRC computer code, the acoustic mode characteristics of multi-layer structures can be calculated. This code is useful for identifying the mode type based upon the comparison of predicted and observed acoustic velocities for surface Rayleigh waves, surface shear waves, and generalized Stoneley waves. Acoustoelectric coupling coefficients for these modes are also predicted by the code.

TABLE 6-1

Summary of Principal Results

Device Configuration	Acoustic Wave Mode	Strain Sensitivity Parallel $\gamma_1 - 1$	Strain Sensitivity Transverse γ_2	1st Order Temperature Coefficient (ppm/°C)	2nd Order Temperature Coefficient (ppm/°C^2)
36°YZ′-Quartz	SSBW	-0.05	1.00	0.0 @ 40°C	0.072
STZ′-Quartz	SSBW	0.045	1.36	-31	---
SiO_2/YX-$LiNbO_3$	SH	-.2	-.3	0.0 @ 51°C	0.21
SiO_2/128°YX-$LiNbO_3$	GSW	<.2	<.2	0.0 @ 50°C	0.044
SiO_2/126°YX-$LiTaO_3$	GSW	-0.2	0.1	---	---

Z′-axis lies in the plane of the substrate and is perpendicular to the X-axis.

TABLE 6-2

SUMMARY OF PROPERTIES OF SELECTED CONFIGURATION

Acoustic Propagation Mode	SSBW
Substrate Configuration	36° Y Quartz
Thin Film Overlay	None
Propagation Direction	Perpendicular to x-axis
Temperature Coefficient	
First Order (ppm/°C)	0 (at 40°C)
Second Order (ppm/°C^2)	0.072
Strain Sensitivity (GF)	
Parallel (γ_1-1)	1.0
Perpendicular (γ_2)	-0.05
Fluid Loading Losses	< 12 dB
Overall Losses	< 20 dB

7.0 REFERENCES

1. Stoneley, R.: Elastic Waves at the Surface of Separation of Two Solids. Proc. Roy. Soc. London, Series A 106, pp. 416-628, 1924.

2. Yamanouchi, K., K. Iwahashi, and K. Shibayama: Piezoelectric Acoustic Boundary Waves Propagating Along the Interface Between SiO_2 and $LiTaO_3$. IEEE Trans. on Sonics and Ultrasonics, Vol. SU-25, No. 6, p. 384-389, November 1978.

3. Shibayama, K., K. Yamanouchi, and W. Chujo: SAW and Boundary Wave Properties for $SiO_2/LiTaO_3$ Structure Fabricated by Plasma-CVD. Proc. IEEE Ultrasonics Symposium, p. 455-459, 1980.

4. Rokhlin, S., M. Mefets, and M. Rosen: An Elastic Interface Wave Guided by a Thin Film Between Two Solids, J. Appl. Phys., 51, p. 3579-3582, July 1980.

5. Browning, T. and M. Lewis: New Family of Bulk-Acoustic-Wave Devices Employing Interdigital Transducers. Electronics Letters, Vol. 13, pp. 128-130, 1977.

6. Yen, K., K. Wang, and R. Kagiwada. Efficient Bulk Wave Excitation on ST Quartz. Electronics Letters, Vol. 13, pp. 37-38, 1977.

7. Yen, K., K. Lau, and R. Kagiwada: Recent Advances in Shallow Bulk Wave Devices. Proc. IEEE Ultrasonics Symposium, p. 766-785, 1979.

8. Yen, K., K. Lau, and R. Kagiwada: Temperature Stable Shallow Bulk Acoustic Wave Devices. Proc. 32nd Annual Symposium on Frequency Control, p. 95-101, 1978.

9. Scholte, J.: The Range of Existance of Rayleigh and Stoneley Waves, Roy. Astron. Soc. London, Monthly Notices Geophys. Suppl., 5, p. 120-126, 1947.

10. Grudkowski, T. and M. Gilden: Realization of Temperature-Compensated GaAs Surface Acoustic Wave Delay Lines, Appl. Phys. Lett., 38, p. 412, 1981.

11. Parker, T. and M. Schultz: SiO_2 Film Overlays for Temperature-Stable Surface Acoustic Wave Devices, Appl. Phys. Lett., 26, p. 75, 1975.

12. Cullen, D., and T. Reeder: Measurement of SAW Velocity Versus Strain on YX and ST Quartz. Proc. IEEE Ultrasonics Symposium, pp. 519-522, 1975.

13. Timosheuko, S. and S. Woinowsky-Krieger: Theory of Plates and Shells, McGraw-Hill, 1959.

14. Sinha, B. and H. Tiersten: On the Influence of Flexural Biasing State on the Velocity of Piezoelectric Surface Waves. Wave Motion, Vol. 1, pp. 37-51, 1978.

15. Stokes, R.: The Effect of Uniform Static Strain on Surface Acoustic Wave Velocity. Ph.D. Thesis, U. of Southern Calif., 1977.

16. Jones, W. R., W. R. Smith and D. Perry: Numerical Computation of Acoustic Surface Waves in Layered Piezoelectric Media-Computer Program Descriptions. AFCRL Rept. FR71-14-102, prepared by Hughes Aircraft Company, February 1971.

17. Kennett, B. L. N.: Elastic Wave Propagation in Stratified Media. In Adv. in App. Mechanics, Vol. 21, p. 79, Academic Press, New York, 1981.

18. Fahmy, A.: Acoustic Wave Propagation and Amplification in Multilayers. Doctoral Thesis, McGill University, 1973.

19. DeRusso, P. M., R. J. Roy and C. M. Close: State Variables for Engineers. Chapter 4-6, John Wiley & Sons, N. Y., 1967.

20. Lewis, M: Surface Skimming Bulk Waves, SSBW. Proc. IEEE Ultrasonics Symposium, p. 744 (1977).

8.0 Publications and Presentations

8.1 Publications

"Surface and Interface Acoustic Waves in SiO /YX-LiNbO " by D. Cullen, G. Meltz, and T. Grudkowski - submitted to Applied Physics Letters

"Acoustic Wave Modes in SiO /128 YX-LiNbO " by D. Cullen, G. Meltz, and T. W. Grudkowski - to be submitted to Applied Physics Letters

8.2 Presentations

"Investigation of the Strain Sensitivity of Subsurface Acoustic Wave Modes" by D. Cullen, G. Meltz, and T. Grudkowski - presented at the 1982 IEEE Ultrasonics Symposium in San Diego, California in October, 1982.

"Surface and Interface Waves in SiO /LiNbO " by D. Cullen, G. Meltz, and T. Grudkowski - to be presented at 1983 IEEE Ultrasonics Symposium in Atlanta, Georgia in October, 1983.

9.0 List of Professional Personnel

Program Manager

T. W. Grudkowski - Manager, Semiconductor Research Laboratory - Ph.D. in Electrical Engineering at Stanford University, 1975 - thesis title "Active Acoustic Waves and Electrons in Gallium Arsenide"

Principal Investigator

D. E. Cullen - Research Scientist, Microelectronics Ph.D. in Physics at the University of Illinois, 1970 thesis titled "Tunneling Spectroscopy in P-Type Silicon"

Theoretical Modeling

G. Meltz - Principal Systems Analyst, Electromagnetics Systems Analysis Group

Program Consultant

G. K. Montress - Principal Scientist, Microelectronics Ph.D. in Electrical Engineering at Massachusetts Institute of Technology, 1976 - thesis title "Fabrication and Large-Signal Characteristics of Baritt Diodes"

APPENDIX A

PREPRINT OF PAPER SUBMITTED

TO APPLIED PHYSICS LETTERS

Surface and Interface Acoustic Waves

In SiO_2/YX-$LiNbO_3$

By

D. E. Cullen, G. Meltz, and T. W. Grudkowski
United Technologies Research Center
East Hartford, CT 06108

Submitted To

Applied Physics Letters
August, 1983

Surface and Interface Acoustic Waves In SiO_2/YX-$LiNbO_3$*

D. Cullen, G. Meltz, and T. Grudkowski
United Technologies Research Center
East Hartford, CT 06108

ABSTRACT

For Y-cut lithium niobate, a leaky shear horizontal (SH) surface wave is known to propagate along the X-axis. When an SiO_2 film is deposited on the $LiNbO_3$ surface, the SH wave is found experimentally to have low loss and theoretical calculations show the wave to be closely confined to the surface. Two additional acoustic modes are observed in the SiO_2/YX-$LiNbO_3$ configuration. One mode is a Rayleigh-type surface wave and the other a generalized Stonely wave. Experimental measurements and theoretical predictions of the wave velocities versus film thickness to wavelength ratio (h/λ) are presented. Measurements of the temperature coefficient of time delay are given for the SH wave showing a zero first order coefficient at $h = .42\lambda$. The sensitivity of this wave to bending strains is also presented.

*Research sponsored in part by the Air Force Office of Scientific Research (AFSC), under Contract F49620-82-C-0074.

Surface and Interface Acoustic Waves

In SiO_2/YX-$LiNbO_3$

D. Cullen, G. Meltz, and T. Grudkowski
United Technologies Research Center
East Hartford, CT 06108

Substrate configurations which support acoustic wave modes having low environmental sensitivity are of interest for achieving stable operating characteristics. In practical device applications, thermal and mechanical stability, related to mounting of the substrate on a rigid carrier, are of primary concern. Generally, stable surface acoustic wave (SAW) devices have utilized Rayleigh waves on substrates that have been chosen primarily for their low thermal sensitivity. In the present work, the SAW of interest is a horizontally polarized shear wave (SH) propagating on a substrate consisting of a deposited SiO_2 film on Y cut $LiNbO_3$, with propagation along the X direction. This wave is shown to provide a zero first order temperature coefficient of time delay and low strain sensitivity under the proper choice of SiO_2 layer thickness. Use of the SH wave has an additional advantage compared to the Rayleigh wave in that sensitivity to surface loading or contaminants is reduced because compressional waves are not radiated into the fluid above the free surface. In addition to the SH polarized SAW, a Rayleigh wave and a Stoneley-like interface wave were also observed.

Processing of devices for this work involved formation of a delay line pattern on a $LiNbO_3$ substrate and deposition of a SiO_2 film over the patterned substrate. Several interdigital transducer designs were employed, including both single and double electrode designs with wavelengths of 12,

16, and 24 microns. The transducers were defined on the $LiNbO_3$ substrate by ion milling of an rf-sputtered Ti/Au/Ti metallization through a photoresist mask. The silica film was also deposited by rf-sputtering in an Ar atmosphere at a temperature of 200°C.

Propagation velocities, particle displacement profiles, and leaky wave attenuations of the various ultrasonic waves supported by the layered structure were calculated as a function of the SiO_2 thickness to wavelength ratio, h/λ, using a transfer matrix formulation of the multi-layer problem.[1] Values of the coupling constant, $K^2 = 2\Delta V/V$, were also determined analytically by computing the propagation velocity with and without a massless metal shorting plane at the SiO_2-$LiNbO_3$ interface.

Figure 1 is a plot of phase velocity versus SiO_2 thickness showing the calculated curves and experimental data points for the Rayleigh wave, the horizontally polarized surface shear wave, and an interface wave which we designate as a generalized Stoneley wave (GSW). The figure covers the range $h/\lambda = 0$ to 1, corresponding to the range of the experiments.

In the case of an electrically shorted interface (Fig. 1-solid curve), a very thin SiO_2 layer is sufficient to transform the SH leaky surface wave[2] into a SH bound mode. If the interface is not metallized (Fig. 1-dashed curve), then a much thicker layer ($h > 0.405\lambda$) is required to load the substrate and prevent the radiation of the veritcally polarized transverse (SV) bulk mode. It can be seen that the coupling constant K^2 can be quite large close to the cut-off of the SH mode. Penunuri and Lakin[3] also found

that a thin oxide film will load an anisotropic substrate and give rise to a strongly coupled piezoelectric Love mode. As the thickness of the oxide layer is increased, the velocity of the SH mode approaches the silica shear velocity value of 3763 m/s.

Figures 2a and b show calculated particle displacement profiles for the horizontal shear SAW and the generalized Stoneley wave at selected values of h/λ with a gold metallized interface surface. The SH wave resembles a pure Love wave with very little motion in the sagital plane, and is tightly confined to the surface wave as indicated by the rapid decay of amplitude with depth. The GSW, in contrast to the SH wave, is concentrated at the vicinity of the SiO_2-$LiNbO_3$ interface with the displacements dominated by the vertical shear (SV) component of polarization. The amplitudes of the GSW at the free surface of the SiO_2 film decrease in magnitude, relative to the amplitude at the interface, as the SiO_2 thickness is increased, so that the wave becomes better confined to the vicinity of the interface as h/λ increases. With a one wavelength thick film, the amplitude of the SV component of the GSW is about three times the surface value. Although, the Scholte Stoneley wave existence conditions[4] are nearly fulfilled for the combination of an SiO_2 layer on YX-$LiNbO_3$, the GSW mode is not as strongly concentrated at the interface as it is in the case of a thick SiO_2 layer on rotated Y-cut $LiTaO_3$.[5] The GSW is cut-off at $h/\lambda = 0.55$ with a metallized interface and at $h/\lambda = 0.66$ without an electrical short at the boundary. If the layer is thinner than the cut-off condition, then an SV bulk wave is radiated, and the large leaky wave attenuation causes the wave to be rapidly damped. The maximum GSW coupling constant K^2 has a value of 0.76% and occurs near $h/\lambda = 0.7$.

Comparing the experimental data points for the Rayleigh-type SAW with theory in Fig. 1 shows that the experimental velocity is always less than predicted. The theoretical curves do not take into account the loading of the metal fingers of the transducer (TiAuTi thickness $\sim 0.01\lambda$). When the metal loading is taken into account, it is found that the velocity is decreased by less than 5 m/*sec* and, therefore, this effect does not account for the difference between theoretical and experimental values. The discrepancy is thought to be related to stresses in the rf sputtered SiO_2 films and the inability to properly model the elastic properties of the SiO_2 films. The GSW is observed only for values of $h > 0.6\lambda$, and calculations show this mode to be cut-off and very lossy for thinner SiO_2 layers.

The SH mode is most interesting because it can be temperature compensated and it has rather low strain sensitivity. Differences between experimental and theoretical velocities in Fig. 1 can again be attributed to metal loading and differences between the real and assumed values of the SiO_2 elastic properties. At $h \approx 0.42\lambda$, the calculated value of K^2 is 7.1% indicating that the mode is easily excited.

The temperature coefficient of delay (TC) was determined experimentally for the SH mode as a function of h/λ. Because of the TC's of SiO_2 and $LiNbO_3$ are opposite in sign, it was expected that a zero value of the TC would be found for some value of h/λ between 0 and 1. Figure 3 shows

the results of the experimental measurements. The SH mode exhibits a zero value of TC (at 20°C) at $h = 0.42\lambda$, and the TC is seen to be a rapidly varying function of h/λ in the vicinity of the zero. The second order TC was found to be 2.1×10^{-7} at $h = 0.42\lambda$.

The sensitivity of the SH mode to bending strain was also measured. An apparatus which can be used to load the $SiO_2/LiNbO_3$ substrate in a cylindrical bending configuration[6] was used in experiments to determine the effects of strain, S, on the frequency, f, of a SH wave oscillator. The effects of strains parallel and perpendicular to the X propagation axis were determined. When strain measurements were made on samples with $h = 0.4\lambda$, the strain sensitivity, defined as $(1/f)(df/dS)$, was found to be quite low. The sensitivities were -0.2 for parallel strains and -0.1 for perpendicular strains. SAW devices on YX or STX quartz have strain sensitivities with magnitudes of 1.0 or greater[6], so that the present $SiO_2/YX\text{-}LiNbO_3$ SH wave delay line is nearly an order of magnitude less sensitive to bending strains.

The reduced sensitivity of the SH-SAW to surface contamination, as compared to the Rayleigh-SAW, was confirmed by coating the surface of the device with a silicone oil and noting the change in insertion loss. While the Rayleigh-SAW was completely absorbed, the insertion loss of the SH-SAW increased by only 3 to 10dB for a number of samples.

In conclusion, we have studied the acoustic wave properties supported by a layered SiO_2/YX-$LiNbO_3$ substrate. For the firt time, a non-leaky shear horizontally polarized surface wave has been found for this structure. At the appropriate SiO_2 layer thickness, this wave possesses a zero first order temperature coefficient, high coupling coefficient, and low sensitivity to bending strains and surface contamination, making it a useful candidate for stable SAW device application.

The authors wish to thank R. Basilica for fabricating the experimental devices, S. Sheades for assitance with electrical measurements, Prof. E. Adler of McGill University for making the initial multi-layer computer code available and M. Page for assistance with the computations.

REFERENCES

1.) A. H. Fahmy and E. L. Adler, Proc. IEE 5, 470 (1975

2.) K. Yamanouchi and K. Shibayama, J. Appl. Phys., 43, 856 (1972)

3.) D. Penunuri and K. M. Lakin, Proc. of the IEEE Ultrasonic Symposium 329, 1972)

4.) J. G. Scholte, Mon. Nat. Roy. Astron. Soc., Geophys. Suppl. 5, 120 (1947)

5.) K. Yamanouchi, K. Iwahashi, and K. Shibayama, IEEE Trans. Sonic and Ultrasonic, SU-25, 348 (1978)

6.) K. Yamanouchi and K. Shibayama, J. Appl. Phys., 43, 856 (1972)

FIGURE 1. PHASE VELOCITY VERSUS SiO_2 THICKNESS FOR SiO_2/YX-$LiNbO_3$

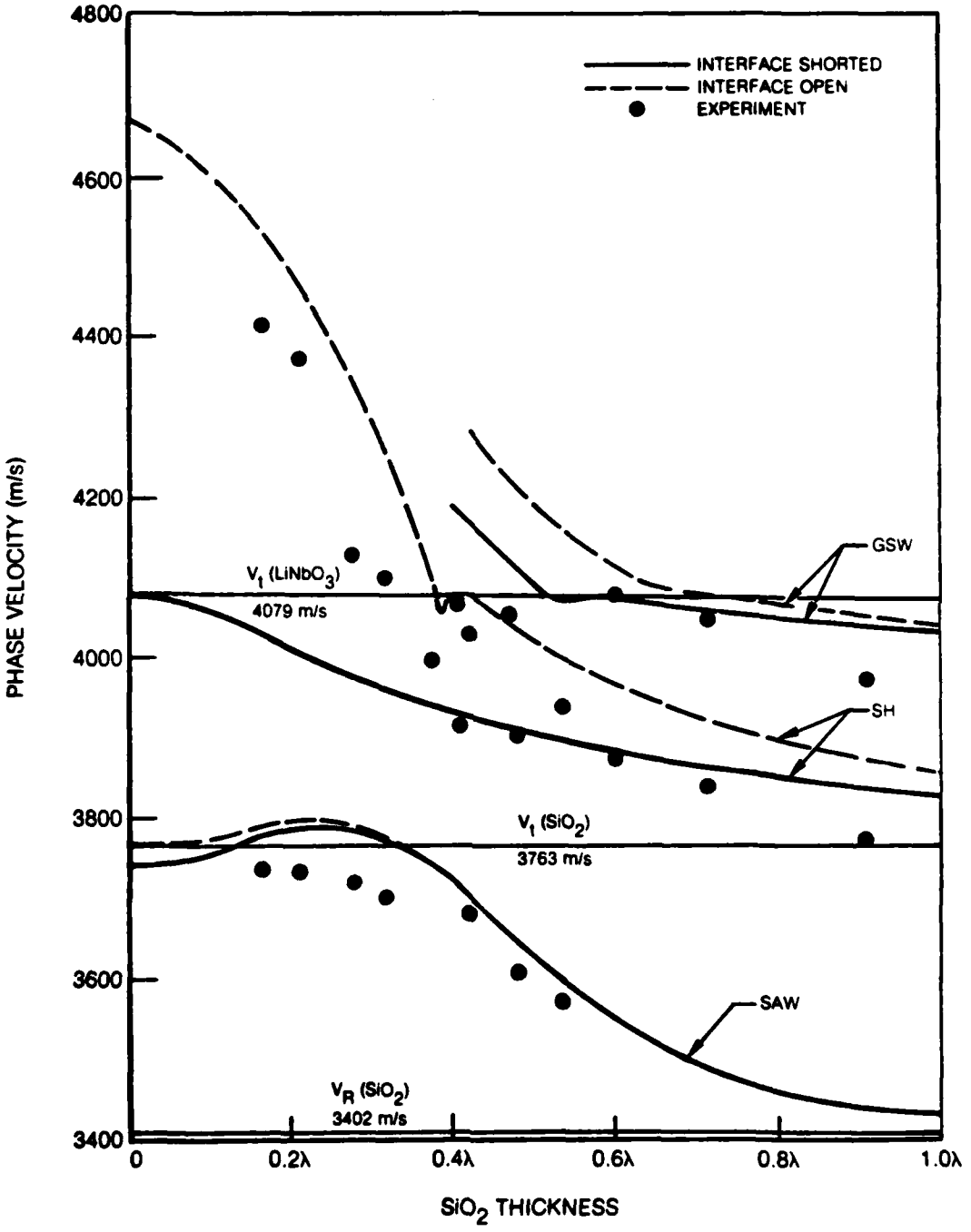

83-4-34-1

FIGURE 2. PARTICLE DISPLACEMENT COMPONENTS FOR SH-SURFACE AND GSW-INTERFACE WAVES

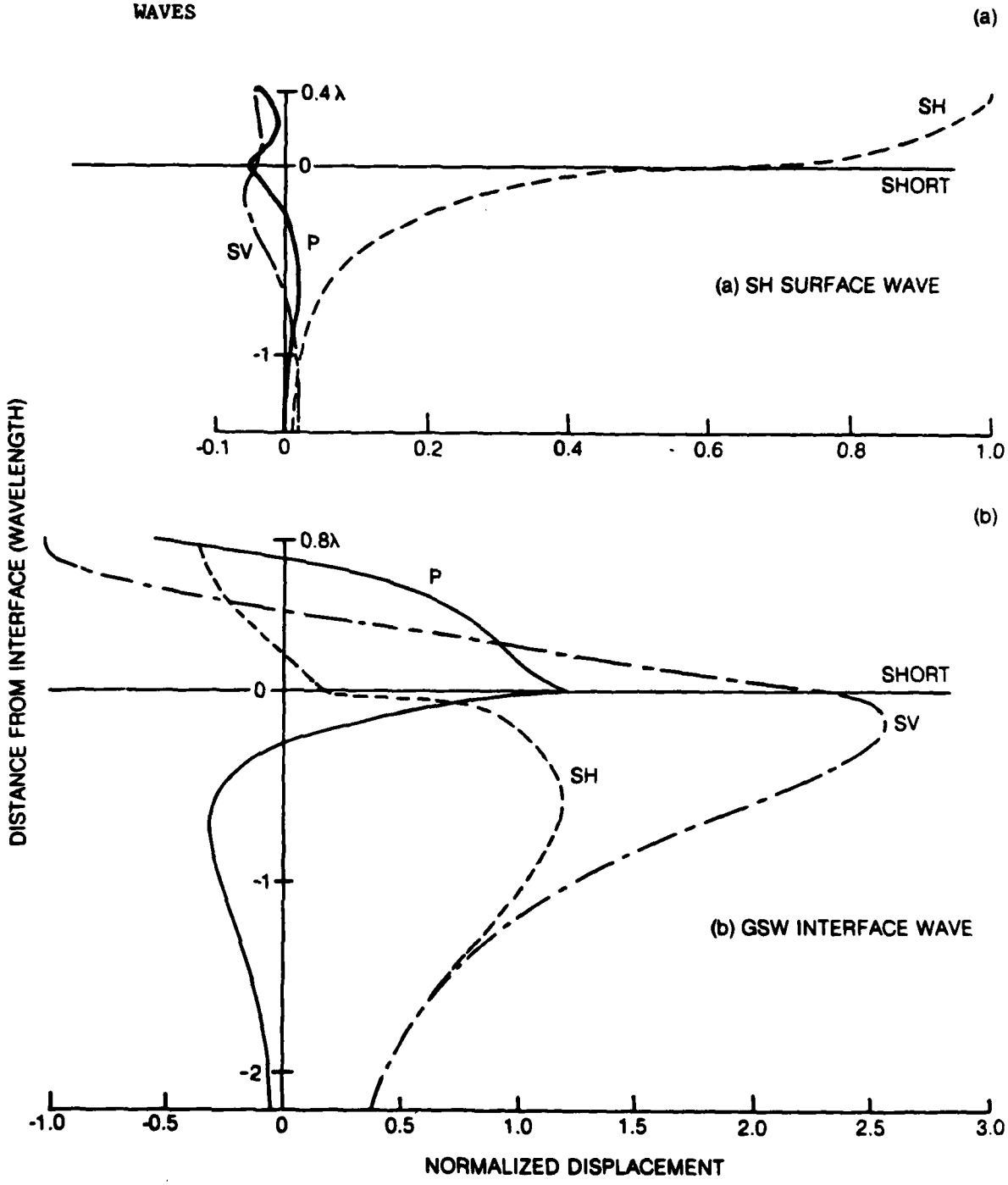

83-8-22-1

FIGURE 3. TEMPERATURE COEFFICIENT VERSUS SiO_2 THICKNESS FOR SH-SURFACE WAVE

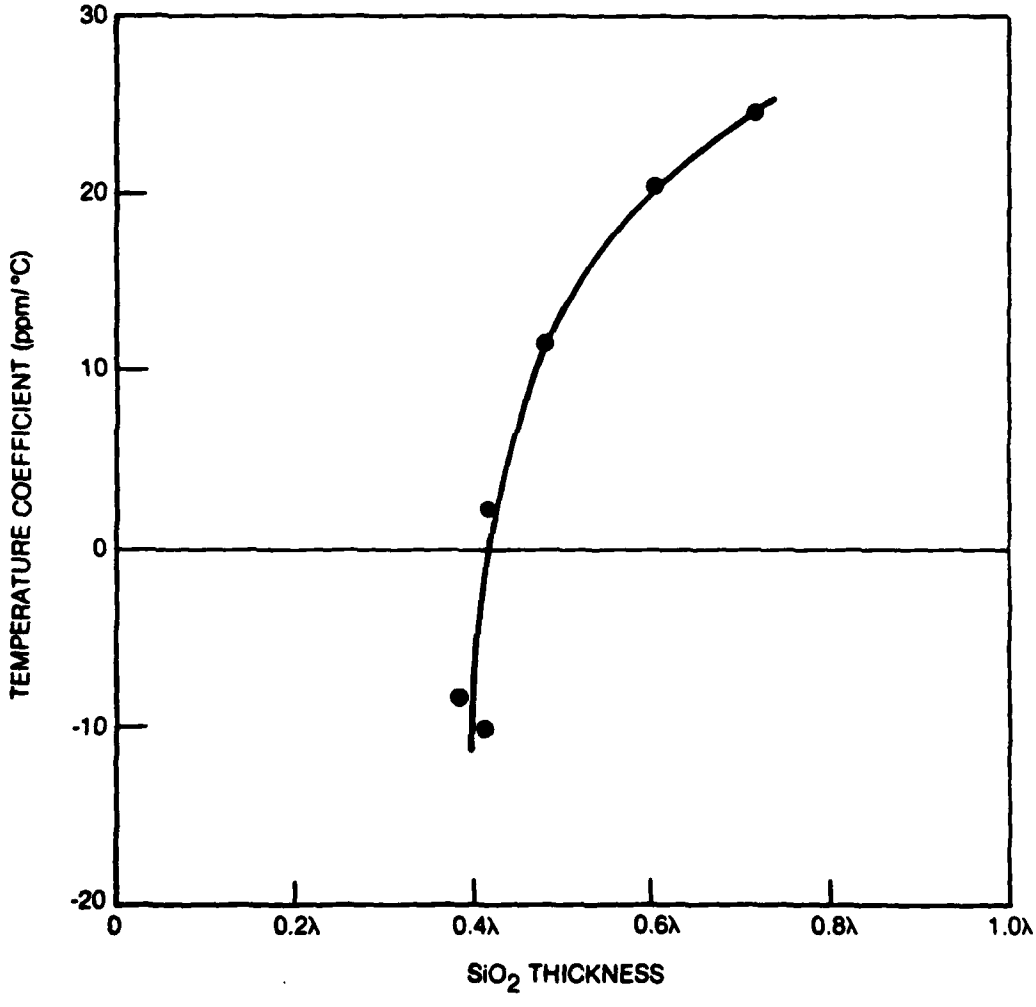

83-4-34-2

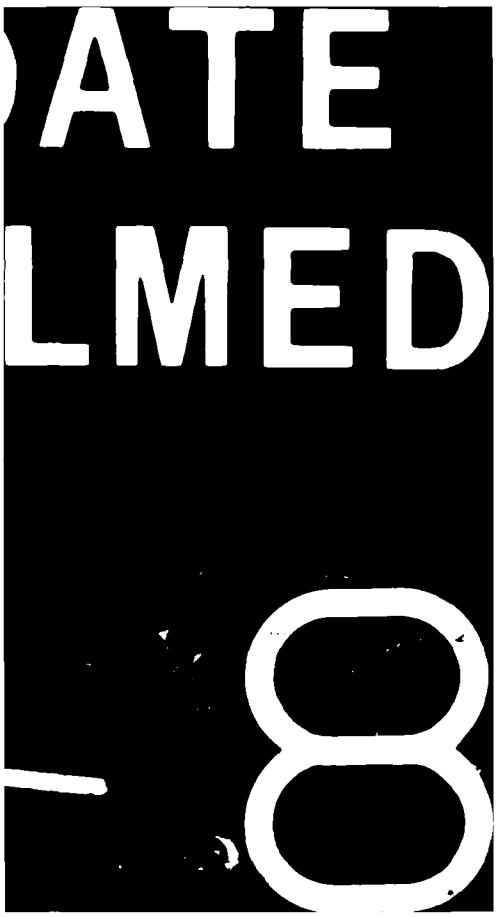
ATE
LMED
8